Bulletin of the Mineral Research and Exploration

http: / / bulletin.mta.gov.tr

Geochemistry of Miocene evaporites from the Aşkale (Erzurum, Eastern Turkey) area: constraints for paleo-environment

Emel ABDİOĞLU YAZAR[a*], Mehmet ARSLAN[a], Cahit HELVACI[b], İbrahim GÜNDOĞAN[b], İrfan TEMİZEL[a] and Didem AYDINÇAKIR[a]

[a] *Karadeniz Technical University, Department of Geological Engineering, 61080, Trabzon, Turkey*
[b] *Dokuz Eylül University, Department of Geological Engineering, Buca 35160, İzmir, Turkey*

Research Article

Keywords:
Evaporite, Gypsum, Anhydrite, Geochemistry, Aşkale, Turkey.

ABSTRACT

The Aşkale sub - basin hosts Early Miocene evaporites intercalated with clastic sediments and carbonates. Gypsum - and anhydrite - rich evaporite samples are characterized by high CaO and SO_4 contents, and low Na_2O, K_2O, MgO, and B contents. The Sr contents are 228 - 13100 ppm in evaporite samples, 169 - 992 ppm in claystone, 181 - 60090 ppm in marl, and 15150 ppm in limestone. All the samples are also characterized by enrichment in light rare earth elements (REE) with La_N / Lu_N = 0.667 - 4.243 and have variable Ce_N / Ce^* (0.823 - 1.353) ratios. Measured Eu_N / Eu^* values of the samples display strong and variable negative and positive Eu anomalies. $\delta^{34}S_{CDT}$ and $\delta^{18}O$ values of gypsum - and anhydrite samples have wide ranges from 21.30 ‰ to 25.62 ‰, and 11.5 ‰ to 19.1 ‰, respectively. Most of these values are heavier than expected Miocene marine gypsum composition and may be resulted from reduction and oxidation reactions of sulfide species in brines. $^{87}Sr / ^{86}Sr$ ratios range from 0.707475 (Δ_{SW} = −169.8) to 0.708175 (Δ_{SW} = −99.8), close to and / or slightly lower than an Early - Miocene marine isotopic composition. Petrochemical and isotopic data indicate that the Aşkale basin evaporites developed in subtropical conditions via multiple marine transgressions onto a shallow platform or lagoonal environment.

Received Date: 15.05.2020
Accepted Date: 21.07.2020

1. Introduction

Facies analysis combined with mineralogic and petrographic examination of evaporitic units may elucidate the depositional environments and paleo - climatological conditions at the time of formation of these units (Warren and Kendall, 1985; Warren, 2010; Kaspryzk, 2003). In addition, discrimination between marine and non - marine origins for ancient evaporites requires consideration of bulk - rock chemistry and sulfur, oxygen, and strontium isotope data (Toulkeridis et al., 1998; Lu et al., 2003; Palmer et al., 2004).

The stratigraphy, mineralogy, and geochemistry of evaporitic units in Neogene basins in Western and Central Anatolia (Turkey) have been investigated by many researchers (Helvacı and Yağmurlu, 1995; Tekin, 2001; Çiner et al., 2002; Orti et al., 2002; Türkmen, 2004; Gündoğan et al., 2005, 2008; Yeşilova, et al., 2018). Further, sulfur, oxygen, and strontium isotope compositions of Cenozoic evaporites from Turkey were reported in detail by Palmer et al. (2004). In the Eastern Anatolia region, the studies of different basins have revealed valuable

Citation Info: Abdioğlu Yazar, E., Arslan, M., Helvacı, C., Gündoğan, İ., Temizel, İ., Aydınçakır, D. 2021. Geochemistry of Miocene evaporites from the Aşkale (Erzurum, Eastern Turkey) area: constraints for paleo-environment. Bulletin of the Mineral Research and Exploration 165, 113-140.
https://doi.org/10.19111/bulletinofmre.772360

**Corresponding author: Emel ABDİOĞLU YAZAR, abdioglu@ktu.edu.tr*

geochemical data that may explain key tectonic events known to have affected the region, such as closure of the Tethyan Oceans and understanding major climatological changes (Yeşilova, et al., 2018). The Aşkale (Erzurum) sub - basin is located at the border of marine and non - marine evaporitic units (Brinkmann, 1976; Palmer et al., 2004) and exhibits evidence for an active compressional tectonic regime related to collision between the Arabian and Laurasian plates during the Paleocene (?) or Eocene to Lower Miocene (Yılmaz, 1993). Nonetheless, despite this important setting, the evaporitic units in the Aşkale (Erzurum) sub - basin have only been investigated by a few researchers (Sancay, 2005; Abdioğlu et al., 2013, 2015; Aydınçakır, 2013).

The stratigraphy, mineralogy, and depositional environment of evaporitic sequences in the Aşkale (Erzurum) sub - basin in Eastern Anatolia (Turkey) were recently studied in detail by Abdioğlu et al. (2015). In this paper, we expand on this work by presenting the first detailed whole - rock geochemical (major, trace, and rare earth element concentrations) and isotopic ($\delta^{18}O$, $\delta^{34}S_{CDT}$, and $^{87}Sr / ^{86}Sr$) data of the Aşkale evaporites to clarify their mode of origin and time of formation.

2. Geological Setting and Local Geology

Turkey is part of the Alpine - Himalayan orogenic belt, and thus was directly affected by collision between the African - Arabian and Eurasian plates during the Cenozoic. Geologically, it is characterized by four main tectonic units: the Pontides, the Anatolides, the Taurides, and the Border Faults (Ketin, 1966; Figure 1a). From north to south, Eastern Anatolia—where the study area is located—contains three tectonic units: (i) the Pontide unit; (ii) the Eastern Anatolian Accretionary Complex (EAAC), which is covered by Late - Miocene to Quaternary collision - related volcanic units; and (iii) the Bitlis - Pötürge Massif (Şengör, 1980; Keskin, 2003). The EAAC forms part of a large accretionary prism situated between the Pontides and the Bitlis - Pötürge Massif (Şengör, 1980; Şengör et al., 2003). This complex also underlies shallow Eastern - Anatolian Late - Miocene basins that extend in an E - W direction and which formed under N - S - oriented compression (Alptekin, 1973; McKenzi, 1976; Tchalenko, 1977).

The evaporitic units outcropping in the Aşkale (Erzurum) area formed in the Tercan - Aşkale sub - basin, which is one of the shallow Eastern Anatolian basins (Sancay, 2005). Basement rocks in this area comprise Jurassic - Cretaceous volcano - sedimentary and ultramafic rocks, which themselves are overlain by Tertiary basins to the north and northwest (Şahintürk and Kasar, 1970; Tarhan et al., 1992; Şahintürk et al., 1997). The Tertiary sedimentary units—namely the Aşkale formation (Sungurlu, 1971)—exhibit features indicative of a shallow marine depositional environment. In the study area, they comprise a sandstone - mudstone - limestone member, an evaporite member, a gravelstone - sandstone - mudstone member, and a limestone member (Abdioğlu et al., 2015; Figure 1b). The age of the formation was reported as Early to Middle Miocene by Şahintürk (1992) and Middle Miocene by Tekin et al. (2000).

A detailed description of the geology and petrography of the Aşkale evaporites has been made by Abdioğlu et al. (2015). The Aşkale evaporite member mainly contains massive, nodular, nodular - banded, wavy laminated, evenly laminated, laminated - banded, and rare enterolithic and chicken - wire gypsum lithofacies in the form of wedges, pods, and lenses. These are interbedded with gypsum - bearing carbonate and clay - rich strata, implying a sabkha depositional setting within the sub - basin. Petrographically, alabastrine, porphyroblastic, and fibrous textures are common in the evaporites, which are dominated by secondary gypsum alongside minor anhydrite, saponite, illite / smectite, calcite, dolomite, and trace amounts of celestite, epsomite, and lutecite (Abdioğlu et al., 2015).

3. Materials and Methods

Based on stratigraphic, mineralogic, and petrographic characteristics, 58 samples of evaporite, limestone, claystone, and marl collected from various stratigraphic levels of the Aşkale evaporite member (Abdioğlu et al., 2015) were selected for lithochemical studies. Samples were prepared for whole - rock analyses at the Department of Geology, Karadeniz Technical University (Trabzon) by crushing into small fragments using a jaw crusher and then pulverizing using a mild - steel mill to produce rock powders with a grain size of <200 mesh. Evaporitic rocks rich in sulfate minerals were the most difficult to analyze, as

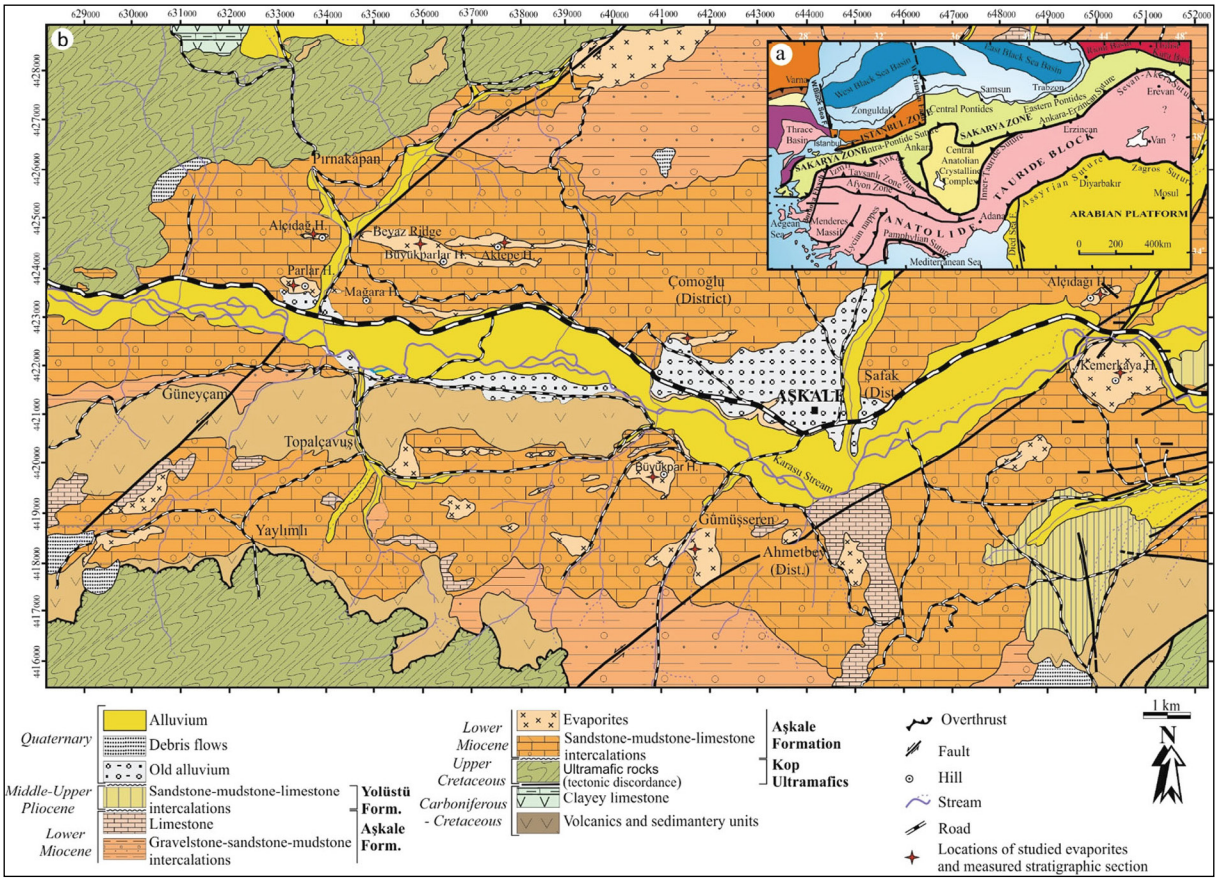

Figure 1- a) Tectonic map of the north-eastern Mediterranean region showing the major sutures and continental blocks (modified after Okay and Tüysüz, 1999). b) Simplified geological map of the Aşkale (Erzurum) sub-basin (modified after Tarhan et al., 1992; Abdioğlu et al., 2015).

each sample had to be ground to 200 mesh to ensure complete fusion of resistant minerals.

Whole - rock analyses were performed at Activation Laboratories Ltd. (Actlabs) in Canada. Whole - rock major, trace, and rare earth element compositions of the 58 samples from different evaporite lithofacies and locations were determined through lithium metaborate / tetraborate fusion with subsequent analysis via inductively coupled plasma optical emission spectrometry (ICP - OES) and mass spectrometry (ICP - MS). Detection limits for major oxides lie within the 0.01 - 0.001 wt. % range. Loss on ignition (LOI) was determined based on weight difference after ignition at 1000 °C. This measured value comprises volatilized H_2O, S, CO_2, organic C, and other weight gains that occur during oxidation of Fe^{2+} to Fe^{3+} but does not include S derived from SO_4 - bearing minerals, as they are non - combustible up to 1050 °C. Detection limits for measured trace and rare earth elements are as follows: 20 ppm for Cr; 5 ppm for V; 2 ppm for Sr and Mo; 1 ppm for Sc, Be, Ba, Ga, and Sn; 0.2 ppm for Sb; 0.5 ppm for Y, Ge, and W; 0.1 ppm for Zr, Rb, In, Bi, Cs, Hf, Co, Ni, Zn, and As; 0.05 ppm for Tl, La, Ce, and Nd; 0.01 ppm for Cu, Pb, Cd, Nb, Ta, Th, Pr, Sm, Gd, Tb, Dy, Ho, Er, and Yb; 0.005 ppm for U and Eu; and 0.002 ppm for Lu and Ag. Analysis of B, Cl, CO_2, and SO_4 contents employed prompt gamma neutron activation (PGNAA), instrumental neutron activation (INAA), infrared (IR), and combustion infrared detection techniques, which have detection limits of 0.5 ppm, 0.01 wt. %, 0.01 wt. %, 0.3 wt. %, respectively.

$\delta^{18}O_{SMOW}$, $\delta^{34}S_{CDT}$ values and ^{87}Sr / ^{86}Sr isotopic ratios were measured in 14 pure gypsum and one anhydrite mineral samples at Activation Laboratories Ltd. (Actlabs) in Canada. The analytical procedures of Kornexl et al. (1999) and Ueda and Krouse (1986) were followed for O and S isotope analysis,

respectively. For Sr isotope ratios, Rb and Sr were separated by extraction chromatography, and then analyzed on a Finnegan MAT 262 multi - collector mass spectrometer. Fifteen simultaneous analyses of SRM - 987 Sr standard runs yielded a weighted average ^{87}Sr / ^{86}Sr value of 0.710258 ± 9 (2s). Based on modern sea water ^{87}Sr / ^{86}Sr value of 0.709173±3 (Denison et al., 1998), Δ_{SW} is defined as $\Delta_{SW} = (^{87}Sr / ^{86}Sr_{sample} - ^{87}Sr / ^{86}Sr_{\text{modern seawater}}) \times 10^{5}$.

4. Results

All geochemical data and statistical analysis as calculated mean, standard deviation and correlation coefficients for the Aşkale evaporites and associated clastic and carbonate rocks from the Pırnakapan (on the Beyaz Ridge), the Alçıdağ hill, the Gümüşseren, and the Kemerkaya sections (Figure 1b) are presented in Supplementary tables 1 - 3. The additional details of the Pırnakapan, the Alçıdağ hill and the Gümüşseren sections as well as petrographic and depositional features of all samples were presented by Abdioğlu et al. (2015).

4.1. Major and Trace Elements

Major oxide variations within the Aşkale evaporites are mainly expressed in terms of varying CaO contents, which are 29.8 - 33.13 wt. % and 40.23 - 41.85 wt. % in the Pırnakapan section for gypsum - rich and anhydrite rich samples, respectively, and 32.19 - 32.59 wt. % in the Kemerkaya section, 30.83 - 33.45 wt. % in the Alçıdağ hill section, and 31.13 - 33.04 wt. % in the Gümüşseren section for gypsum - rich samples. All sulfate mineral - rich samples are characterized by low Na_2O (0.01 - 0.13 wt. %), K_2O (0.01 - 0.29 wt. %), MgO (0.01 - 2.55 wt. %), and Cl (0.01 - 0.04 wt. %) contents (Supplementary Table 1).

Certain trace elements in evaporites (e.g., Li, Br, and B) provide constraints on their paleo - environment of formation and can be used to discriminate between marine and non - marine origins (Warren, 2010). The B contents of the analyzed Aşkale evaporites are very low, with gypsum - and anhydrite - rich samples having 0.8 - 20.3 ppm, limestone having 13.8 ppm, claystone having 74.9 - 76.6 ppm, and marl having 3.5 - 188 ppm. In all cases, measured Br contents are very close to the detection limits (0.01 - 6 ppm, Supplementary Table 1). Measured Ni, Cr, and Co contents vary from sample to sample, with their concentrations being generally higher in associated clastic sediments. The Aşkale evaporites have Sr contents of 228 - 13100 ppm in gypsum rich samples, 1023 - 1197 ppm in anhydrite rich samples, 169 - 992 ppm in claystone, 181 - 60090 ppm in marl, and 15150 ppm in limestone.

Multi - element spider diagrams normalized to MuQ (Mud of Queensland), which represents the composition of weathered, young, upper - continental crust - derived alluvial sediment (Kamber et al., 2005), show that gypsiferous samples are more depleted than claystone - limestone - marl samples (Figure 2). In addition, all evaporite samples are strongly depleted in Rb, Th, and Zr, but have slight enrichment in Ba and a marked enrichment in Sr.

4.2. Bivariate Plots

Relationships between major oxides and selected trace and rare earth elements in the Aşkale evaporites were quantified using correlation coefficients, which were calculated for a significance level of $p < 0.01$ using the Statistica 10 program (Supplementary Table 3). This analysis shows that most elements have strong positive correlations with each other, except CaO, which generally displays a strong negative correlation, while Sr and Ba display very weak correlations.

Bivariate element variation diagrams have much use in identifying the control of mineralogical variations on the bulk geochemistry of an evaporite. The most important major oxides in the Aşkale evaporites are SiO_2 and CaO, which are significant components in authigenic silicate and sulfate minerals, as well as being able to highlight variations in the proportions of diagenetic and / or clastic minerals. To better understand variations between major oxides and trace elements, variation diagrams for SiO_2 versus other major oxides (Figure 3) and SiO_2 versus trace elements (Figure 4) were plotted. These bivariate plots show positive and negative trends between various components. For example, Al_2O_3, TiO_2, K_2O, Fe_2O_{3total}, MgO, Th, Co, Ba, Ce, As, and Ni have a strong positive correlation with SiO_2, whereas CaO and SO_4 show a weak negative correlation. There appears to be a partly negative (but dispersed) relationship between SiO_2 and Sr.

Figure 5 shows Sr vs. Mg, Na vs. Mg, Sr vs. Na, and Sr vs. B element variation diagrams for gypsum

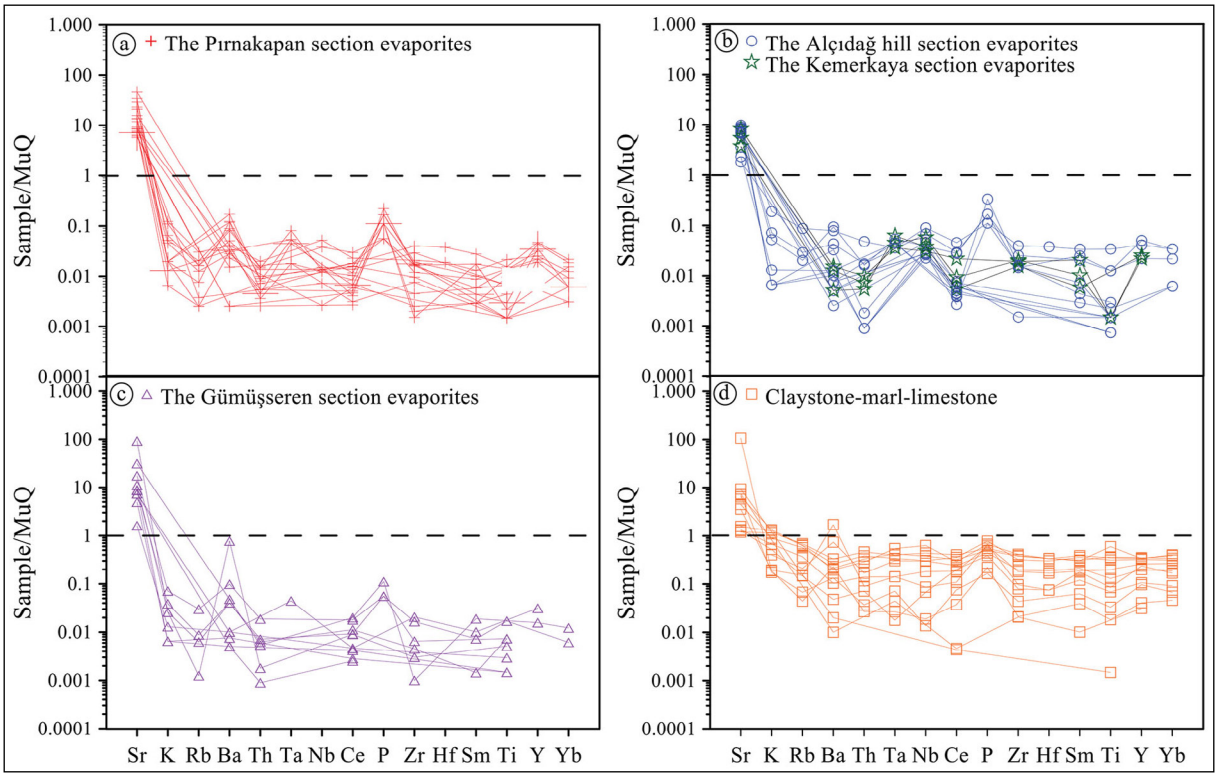

Figure 2- a - d) MuQ-normalized multi-element spider diagrams for the Aşkale evaporites and claystone - marl - limestone. MuQ = Mud of Queensland—an average sediment composition (Kamber et al., 2005).

- anhydrite rich samples from different sections and claystone - limestone - marl samples. These data show that Sr vs. Mg and Sr vs. Na plots have relatively positive trends if claystone - limestone - marl samples not considered but scattered trends in general. Na vs. Mg plot displays a relatively positive trend whereas Sr vs. B plot has a scattered and negative trend (Figure 5).

4.3. Rare Earth Element (REE) Geochemistry

In general, the measured REE contents of the gypsum - anhydrite rich evaporite samples are very low. For example, La contents are in the range 0.08 - 1.97 ppm and Lu contents are in the range 0.002 - 0.019 ppm (Supplementary Table 2). The overall REE concentrations are close to or below their respective detection limits, implying that hydrothermal fluids were not effective during the formation process (Emelyanov and Shimkus, 1986).

All evaporite, claystone, marl, and limestone samples exhibit a generally flat MuQ - normalized REE pattern, with slight enrichment in LREE. La_N / Lu_N ratios are 0.867 - 4.243 for the Pırnakapan section, 2.713 - 4.220 for the Kemerkaya section, 1.349 - 2.488 for the Alçıdağ Hill section, 1.658 for the Gümüşseren section evaporites, and 0.677 - 1.540 for the claystone - marl - limestone samples. All the samples exhibit both positive and negative Ce (0.823 - 1.353) and Eu (0.389 - 2.245) anomalies (Figure 6).

4.4. Isotope Geochemistry

Isotope geochemistry is commonly used to explain the origin, diagenetic conditions, and environment of formation of evaporites. In lithologies containing sulfate minerals, sulfur, oxygen, and strontium isotopes are of critical importance to understand the chemistry and temporal evolution of fluids during precipitation of evaporitic minerals (Müller and Mueller, 1991; Rosell et al., 1998; Ortí and Rosell, 2000; Playà et al., 2000; Palmer et al., 2004; Tekin et al., 2010; Crockford et al., 2019).

Table 1 shows $\delta^{34}S_{CDT}$, $\delta^{18}O$ and ^{87}Sr / ^{86}Sr isotopic ratios for gypsum and anhydrite samples from the Aşkale evaporites. These data highlight that

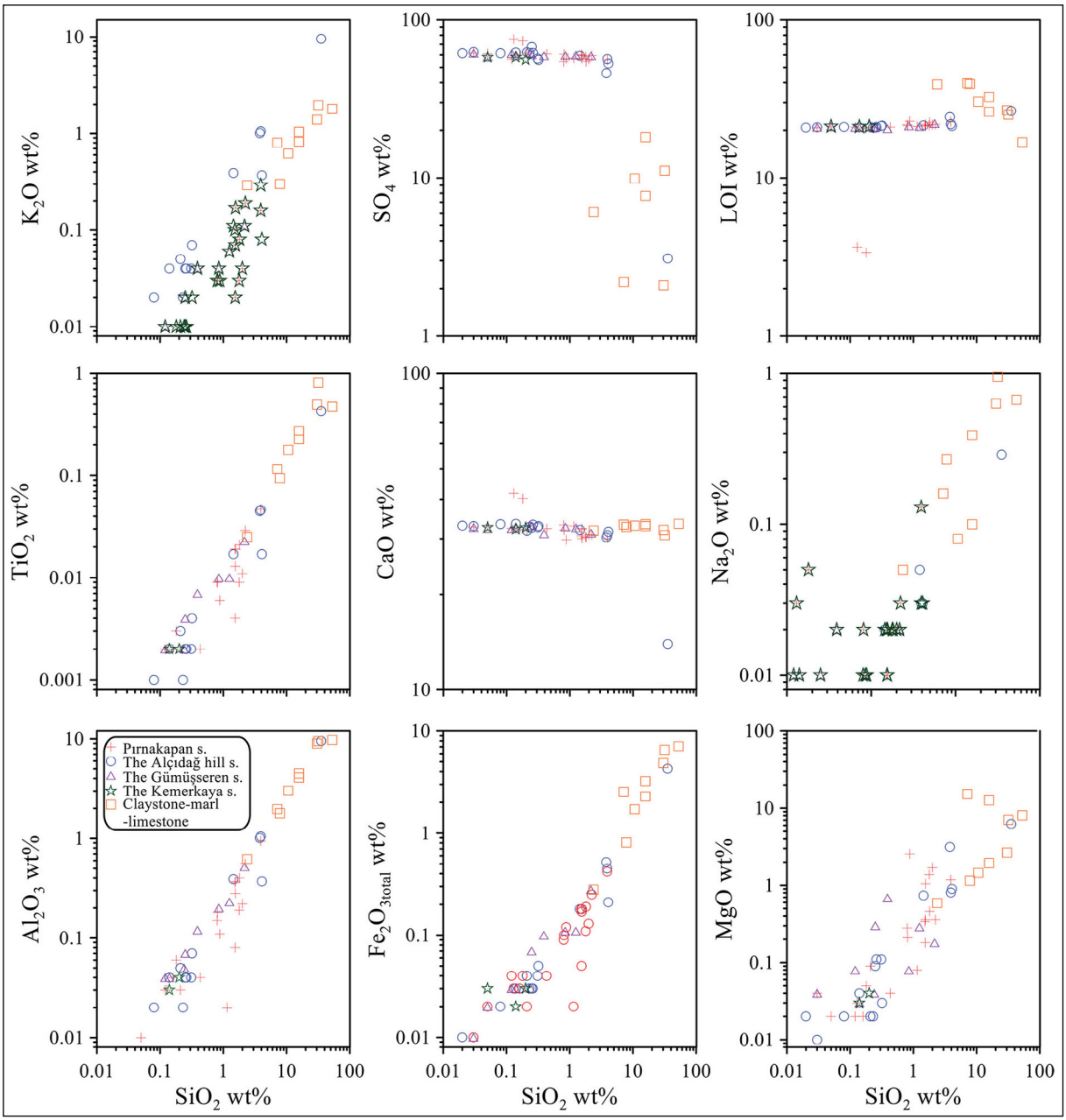

Figure 3- SiO_2 (wt. %) versus selected major element oxide (wt. %) variation plots for the Aşkale evaporites.

the $\delta^{18}O$ isotopic compositions lie within the range 11.5 - 19.1 ‰, with a mean value of 14.67 ‰; the $\delta^{34}S_{CDT}$ isotopic compositions range from 21.3 ‰ to 25.62 ‰, with a mean value of 23.22 ‰; and ^{87}Sr / ^{86}Sr ratios are 0.707475 (Δ_{SW} = −169.8) to 0.708175 (Δ_{SW} = −99.8) (Table 1).

5. Discussion

Determination of the paleo - environment of deposition of the Aşkale evaporites requires combining major, trace, and REE geochemistry with isotopic data. Interpretations of these results are given below.

5.1. Assessment of Whole - Rock Chemical Data

Positive correlations between SiO_2 and other major oxides observed on binary variation diagrams for the Aşkale evaporites (Figure 3, Supplementary Table 1 and 3) indicate that the paleo - depositional environment shallowed due to evaporation, allowing clay or clastic materials to be transported into the

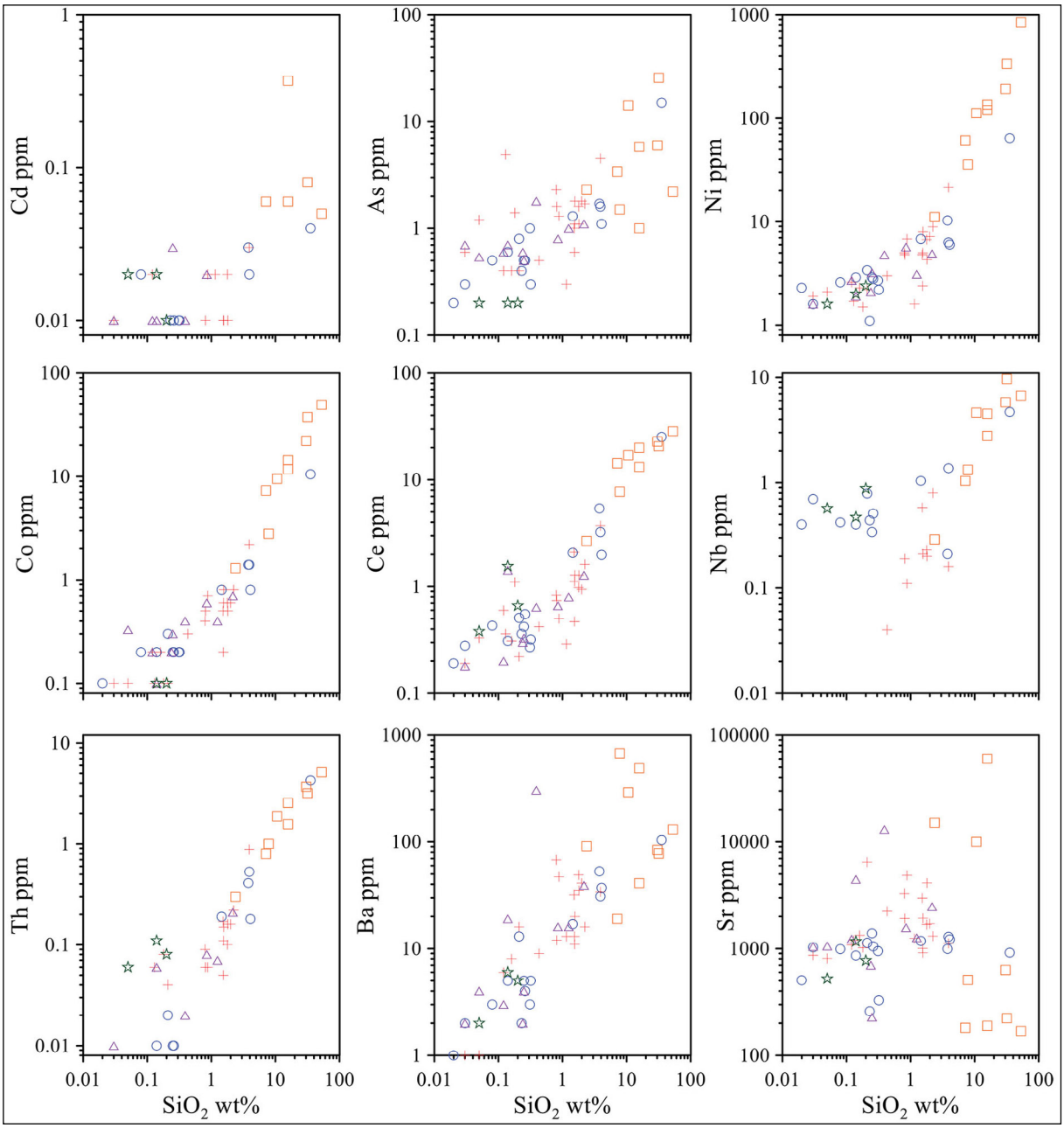

Figure 4- SiO_2 (wt. %) versus selected trace element (ppm) variation plots for the Aşkale evaporites (symbols as in Figure 3).

region from continental sources. Negative SiO_2 - CaO and SiO_2 - SO_4 correlations support this evaporative shallowing hypothesis, as they record reduced precipitation of Ca - sulfate over time (Bahadori et al., 2011). Generally, the poor correlation between SiO_2 and Sr indicates that Sr may have marine source with some continental input. The correlation between SiO_2 and Ba content may be similarly explained via increasing Ba - sulfate and Ba - chloride crystallization during shallowing, likely due to evaporation of the paleo - depositional environment (Bahadori et al., 2011). The low Ba contents of the investigated Aşkale evaporite samples may indicate either input of continental clastic material or, precipitation of barite even under very low Ba concentration (Horner et al., 2017) although barite was never detected by means mineralogical examinations in the Aşkale evaporites.

When binary element variation diagrams are assessed with correlation coefficients (see

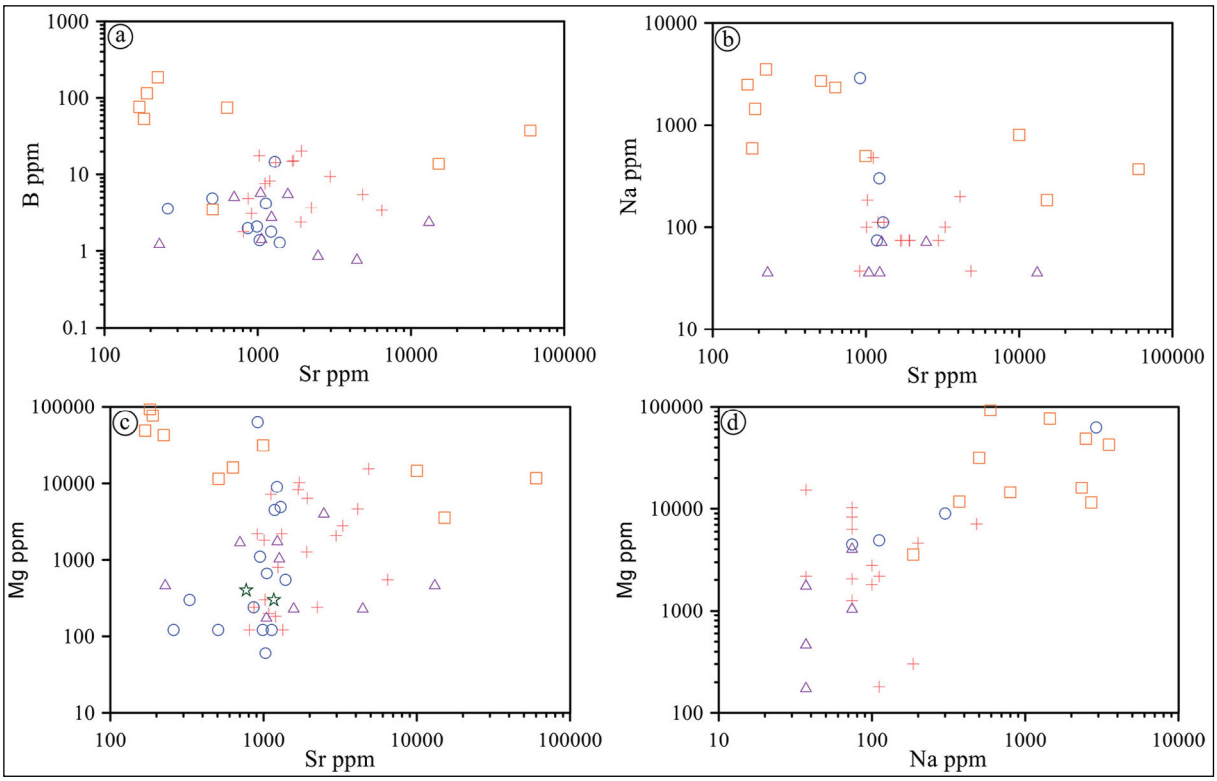

Figure 5- Cross-plots of trace element compositions of the Aşkale evaporites. a) Sr vs. B, b) Sr vs. Na, c) Sr vs. Mg, d) Na vs. Mg (symbols as in Figure 3).

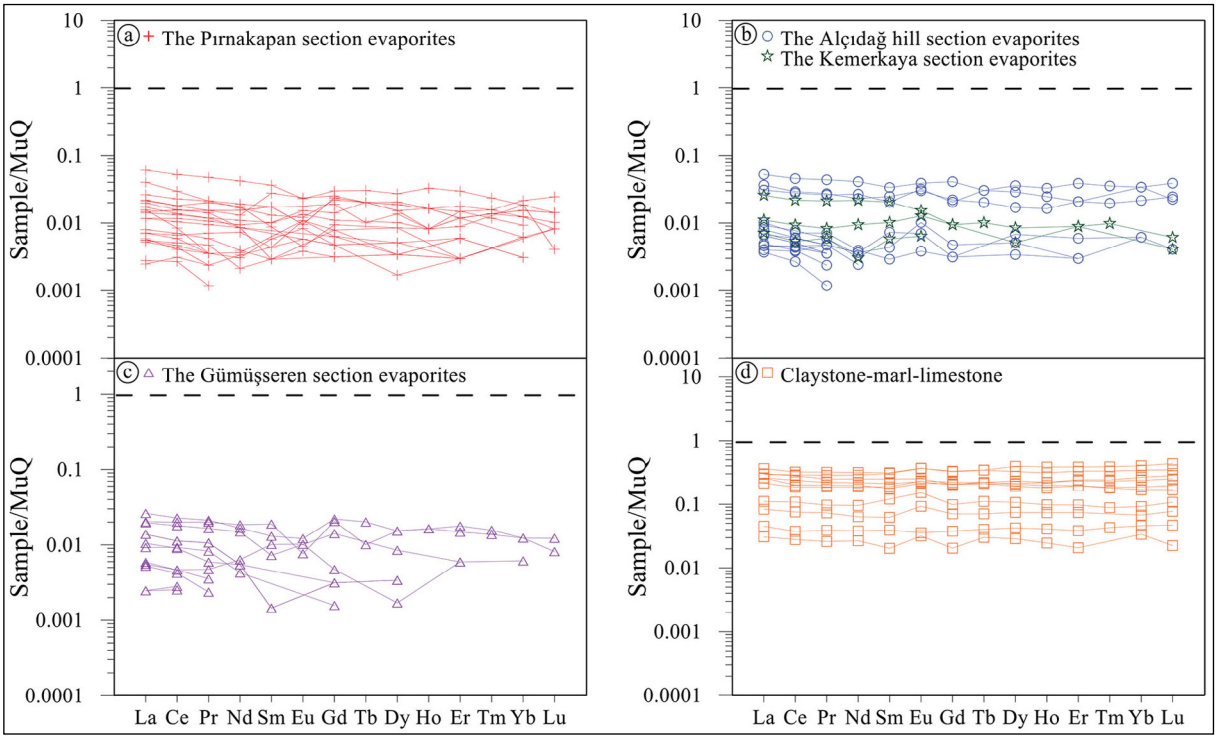

Figure 6- a - d) MuQ-normalized REE patterns for the Aşkale evaporites. MuQ = Mud of Queensland - an average sediment composition (Kamber et al., 2005).

Table 1- $\delta^{18}O_{SMOW}$, $\delta^{34}S_{CDT}$ values, and ^{87}Sr / ^{86}Sr isotopic ratios of gypsum and anhydrite samples from the Aşkale evaporites.

Sample Number	**Section**	**Texture**	**Mineralogy**	**$\delta^{18}O_{SMOW}$** (‰)	**$\delta^{34}S_{CDT}$** (‰)	**^{87}Sr / ^{86}Sr** ±2s	Δ_{SW}
A-1	Alçıdağ hill	nodular	*gypsum*	13.5	22.9	0.707475 ± 4	-169.8
A-6		alabastrine		16.0	23.5	0.707991 ± 5	-118.2
A-11		nodular		12.7	23.4	0.708102 ± 4	-107.1
A-16		alabastrine		13.3	21.3	0.708147 ± 12	-102.6
D1-5	Pırnakapan	laminated		18.0	24.1	0.708076 ± 3	-109.7
D1-28		alabastrine		15.0	22.9	0.708046 ± 4	-112.7
D1-32		alabastrine		14.5	22.9	0.708092 ± 4	-108.1
D3-4		nodular		19.1	23.74	0.707488 ± 8	-168.5
D3-5		laminated		18.8	25.62	0.707480 ± 16	-169.3
K-3	Gümüşseren	alabastrine		14.4	23.6	0.708163 ± 5	-101.0
K-4		alabastrine		11.5	23.23	0.708174± 17	-99.9
K-9		nodular		13.6	22.3	0.708114 ± 5	-105.9
K-14		banded		12.1	22.3	0.708121 ± 3	-105.2
K-25	Kemerkaya	alabastrine		14.1	22.94	0.708175 ± 15	-99.8
D1-22	Pırnakapan	nodular	*anhydrite*	13.5	23.6	0.708144 ± 4	-102.9

Supplementary Table 3), samples containing common sulfate minerals appear to match those with sparse silicate minerals. These silicate minerals are generally accompanied by clay minerals, such as illite and Mg - smectite, and varying proportions of Ni - , Cu - , and Fe - rich minerals. Transportation of clastic material from a continental source region might therefore have occurred in the cycle of evaporite formation, driven by periods of high precipitation that followed dry seasons. This interpretation agrees with constraints imposed by regional geology, as the regression was effective during periods of evaporite formation (Sancay, 2005). Thus, enrichments in Ni, Cu, and Co can be linked to the input of clastic material sourced from the surrounding Kop ultramafic rocks. The positive relationship between SO_4 and CaO results from gypsum and / or anhydrite formation, although SO_4 shows a variably negative correlation with nearly all elements. Importantly, there is no correlation between SO_4 and Sr, as Kushnir (1980, 1982) reported that the increasing evaporation of Sr - rich seawater may drive celestite crystallization simultaneous with gypsum. The presence of epigenetic celestite formed during a late stage of diagenesis was proved by means of petrographical examinations as crack or cavity infillings of micritic limestones and in the secondary gypsum lithofacies accompanying to gypsum and sometimes to lutecite (Abdioğlu et al., 2015). Thus, a high Sr content can be attributed to epigenetic celestite formation.

Figure 5 shows that Sr content has a dispersed and / or negative correlation with B content. Measured B contents in gypsum - rich samples (0.8 - 20.3 ppm), anhydrite - rich samples (8.2 - 17.7 ppm), limestone samples (13.8 ppm), claystone samples (74.9 - 76.6 ppm), and marl samples (3.5 - 188 ppm) show no correlation between it and Sr. In fact, the interpreted increase in clastic material with time appears to relate to a partial increase in B content.

As seawater has a much lower REE concentration than river water (Playà et al., 2007), the REE content of an evaporite is controlled by the input of continental material. Figure 6 shows that regression related Aşkale evaporite samples interpreted to contain clastic material also have high REE contents. Consequently, ultramafic rocks surrounding the paleo - basin should also have high REE contents if they are considered a potential source of detritic material. Clay - rich Aşkale samples have higher REE contents compared to evaporitic samples, and clay and carbonate samples have flat REE distribution patterns, indicating intense chemical differentiation. The REE distributions within evaporite samples are similar in shape but differ in magnitude.

The speciation of Ce and Eu in sedimentary rocks is useful for determining redox states within a depositional environment. Thermodynamic calculations by Sverjensky (1984) indicate that Eu^{2+} is more abundant than Eu^{3+} in high temperature reducing environments. Indeed, minerals precipitating under reducing conditions (Eu^{2+} / Eu^{3+} > 1) generally have a positive Eu anomaly. The Aşkale evaporites have both positive and negative Eu anomalies of varying magnitudes, with Eu_N / Eu* values of 0.389 - 2.245 in gypsum - and anhydrite - rich samples, 0.927 in limestone, 1.045 - 1.396 in claystone, and 1.094 - 1.392 in marl. In Aşkale clastic samples, positive Eu anomalies likely represent the presence of continental sedimentary material. Aşkale samples rich in sulfate minerals show strong negative and positive Eu anomalies, independent of lithofacies, which likely records occasional freshwater input to the depositional environment, with deepening and shallowing periods linked to local climatic and tectonic activity.

Similarly, positive and negative Ce anomalies provide valuable information about the environment of formation. For example, Ce in rocks typically occurs in the 3^+ valence state, but oxidizes over time, and thus enters fluids in the 4^+ valence state. Given that low - temperature seawater - mineral interactions are characterized by high Ce^{4+} / Ce^{3+} ratios in the fluid, rocks affected by such aqueous alteration processes should have a negative Ce anomaly, although if Ce^{4+} is then incorporated into newly formed minerals, rocks should have a positive anomaly (Ludden and Thompson, 1979; Menzies et al., 1979). Thus, the Ce_N / Ce^* values recorded in Aşkale gypsum - and anhydrite - rich samples (0.823 - 1.353), and marl, limestone, and claystone samples (0.873 - 1.045) have both mildly negative and mildly positive Ce anomalies. Such negative Ce anomalies infer the influence of seawater in the paleo - depositional basin.

In evaporites, Sr^{2+} may exchange with Ca^{2+} to form celestite ($SrSO_4$) (Adabi, 2004). Usdowski (1967) indicated that the mean Sr content of seawater that precipitates gypsum is ~1400 ppm, with this value being preserved in the crystals even if gypsum transforms to anhydrite during diagenesis. Evaporites developing in marine environments have a Sr content of 1000 - 3000 ppm (Emelyanov and Shimkus, 1986; Hasselöv et al., 1999), while those developing in continental environments have a Sr content of 50 - 200 ppm (Krauskopf, 1979). Lacustrine Miocene evaporites from north - eastern Spain have Sr contents below 500 ppm with sulfate and chloride ions sourced from adjacent Mesozoic continental salts (Orti et al., 2007). Study of rocks from the East Betik strait, Spain, has shown that normal seawater - derived banded, nodular, and laminated gypsum from Late - Miocene continental and marine evaporites have a Sr content of 800 - 1700 ppm, whereas selenitic and massive gypsum, which form from hydrothermal solutions, have a Sr content of 2400 ppm (Playà et al., 2000). The Aşkale gypsum and anhydrite strata have similar Sr contents to those of strata from the East Betik strait, emphasizing that their constituent minerals formed from seawater (Kushnir, 1980, 1982). In situations where non - marine fluids contribute to evaporite mineral genesis, the compositions of these evaporites may differ significantly from those of evaporites primarily formed from seawater (Usdowski, 1967; Kushnir, 1980, 1982; Rushdi et al., 2000; Symkatz - Kloss and Roy, 2010; Bahadori et al., 2011). The Aşkale evaporites have Sr contents of 228 - 13100 ppm in gypsum - and anhydrite - rich samples and 169 - 60090 ppm in claystone - marl - limestone samples, which most closely resemble marine - sourced evaporites. Gypsum and anhydrite samples with high Sr contents are thought to include Sr^{2+} within their crystal lattices (Tekin, 2001), although high Sr contents are generally thought to denote marine depositional environments. However, it should be considered that simultaneous volcanism around the basin may increase Sr input to environment, resulted in much higher Sr content than normal seawater. Extremely high Sr contents (60090 ppm) are associated with celestite formation, which is very common in carbonate rocks. The source of such enrichment may be related to dissolution of Sr from previously formed gypsum, which may then be precipitated as celestite.

Major and trace element data from evaporites occurred in Neogene basins of Turkey were compared with the gypsum - and anhydrite - rich samples from the Aşkale area (Table 2). The major element contents of the Aşkale evaporites resemble the major oxide values of evaporites from the Ulaş (Sivas) basin (Tekin, 2001) and the Beypazarı and Çankırı - Çorum basins (Gündoğan and Helvacı, 2001; Gündoğan, 2000), but are lower than evaporites in the Central Sakarya basin (Zeybek, 2007) (Table 2). In addition, the Ba, Pb, and Cu contents of the Aşkale evaporites resembles those from evaporites in the Central Sakarya basin but are

much higher than those in evaporites from the Ulaş basin. The Sr contents of the evaporites studied in this work are much higher than those reported by Baysal and Ataman (1980) and Gökçe and Ceyhan (1988) but resemble the results of Tekin (2001) and Zeybek (2007). The Mg content of Aşkale evaporites samples resemble those of Zeybek (2007) but are higher than other studies. As such, the Aşkale evaporites most closely resemble the Ulaş (Sivas) basin evaporites, which are also described as having a marine origin (Tekin, 2001).

5.2. Chemostratigraphic Correlations

The correlation of geochemical variations with stratigraphic level is commonly used to make paleo - climatological interpretations (Bahadori et al., 2011). As such, whole - rock geochemistry was used in combination with measured stratigraphic sections to quantify geochemical variation in the Aşkale evaporites and quantify the types and magnitudes of changes (Figure 7).

Highly soluble ions, such as Na^{+}, Mg^{2+}, and K^{+}, exhibit very different differentiation behaviors compared to stable (insoluble) ions, such as Ti^{4+}, Al^{3+}, and Fe^{3+} (Mason and Moore, 1982). When soluble elements are transported by water, sediments tend to become enriched in insoluble elements. As a result, the relative concentrations of these two ionic groups reflect paleo - environmental conditions (Nesbitt and Young, 1982; Gallet et al., 1996; Roy et al., 2006, 2009). Smykatz - Kloss and Roy (2010) recommended the use of Na_2O / Al_2O_3, Na_2O / Fe_2O_3, Na_2O / TiO_2. and Na_2O / K_2O ratios to decipher the paleo - climatological conditions in which evaporite minerals formed. Of this set, all but Na_2O / K_2O are expected to increase commensurately with an increase in aridity or a reduction in aqueous activity (Bahadori et al., 2011). By contrast, both Na and K are soluble

Table 2- Comparison of major and trace element compositions between some evaporite deposits of Turkey and the Aşkale evaporites.

	Zara-Refahiye Basin	Celali-Karayün-Hafik Basin	Sivas-Ulaş Basin	Beypazarı Basin	Çankırı-Çorum Basin	Middle Sakarya Region	Aşkale Basin
wt%							
SiO_2				0.56 - 3.89	1.14 - 4.97	0.22 - 25.72	0.02 - 3.92
Al_2O_3				0.1 - 0.75	0.26 - 1.15	0.08 -10.72	0.01 -1.05
Fe_2O_3*				0.037 - 0.418	0.135 - 0.693	0.04 - 6.81	0.01 - 0.45
MnO				0.001 - 0.011	0.002 - 0.017	_	0.002 - 0.009
MgO			0.17 - 0.32	0.21 - 7.45	0.14 - 14.73	0.07 - 33.98	0.02 - 2.55
CaO			32.7 - 38.6	2.87 - 39.86	14.13 - 38.62	7.75 - 56.75	29.8 - 41.85
Na2O			0.11 - 0.31	0.004 - 42.38	0 - 0.17	0.06 - 0.27	0.01 - 0.13
K_2O			0.1 - 1.2	0.023 - 0.184	0.051 - 0.315	0.01 - 0.87	0.01 - 0.29
TiO_2				0 - 0.069	0 - 0.069	0.01 - 0.77	0.002 - 0.047
P_2O_5						0.01 - 0.87	0.01 - 0.02
ppm							
Sr	783	2450	2526 - 5368			256.9 - 5270	228-13100
Ba			0.01 -6.5			11.6 - 273.9	1 - 305
Ni						2.2 - 97.1	1.1 - 21.4
B							0.8 - 20.3
Li	2.8	3.1	1.6 - 3				
F	16.1	40	3.4 - 4.8				
Pb			0.14 - 2.5			2 - 20.07	0.04 - 2.12
Cu			0.1 - 2			1 - 43.1	0.41 - 6.07
Mg	3741	6528	3158 - 4768				
Age	Miocene	Miocene	Miocene	Middle-Late Miocene		Miocene	Early Miocene
Environment			Marine	Playa lake		Playa lake	
Reference	Baysal and Ataman (1980)	Gökçe and Ceyhan (1988)	Tekin (2001)	Gündoğan (2000)		Zeybek (2007)	This study

elements, and K is easily adsorbed by sedimentary minerals, such as illite, leading to the formation of new species (Pandarinath et al., 1999). Thus, unless environmental conditions change, the Na_2O / K_2O ratio of an aqueous solution should remain the same (Bahadori et al., 2011).

Figure 7 shows that the Aşkale evaporites have very low Na_2O / Al_2O_3, Na_2O / Fe_2O_3, Na_2O / TiO_2, and Na_2O / K_2O ratios, and there is no significant variation up - section, although Ce_N / Ce^* ratios and Sr contents show minor changes. These data may be explained largely by a non - marine fluid contribution

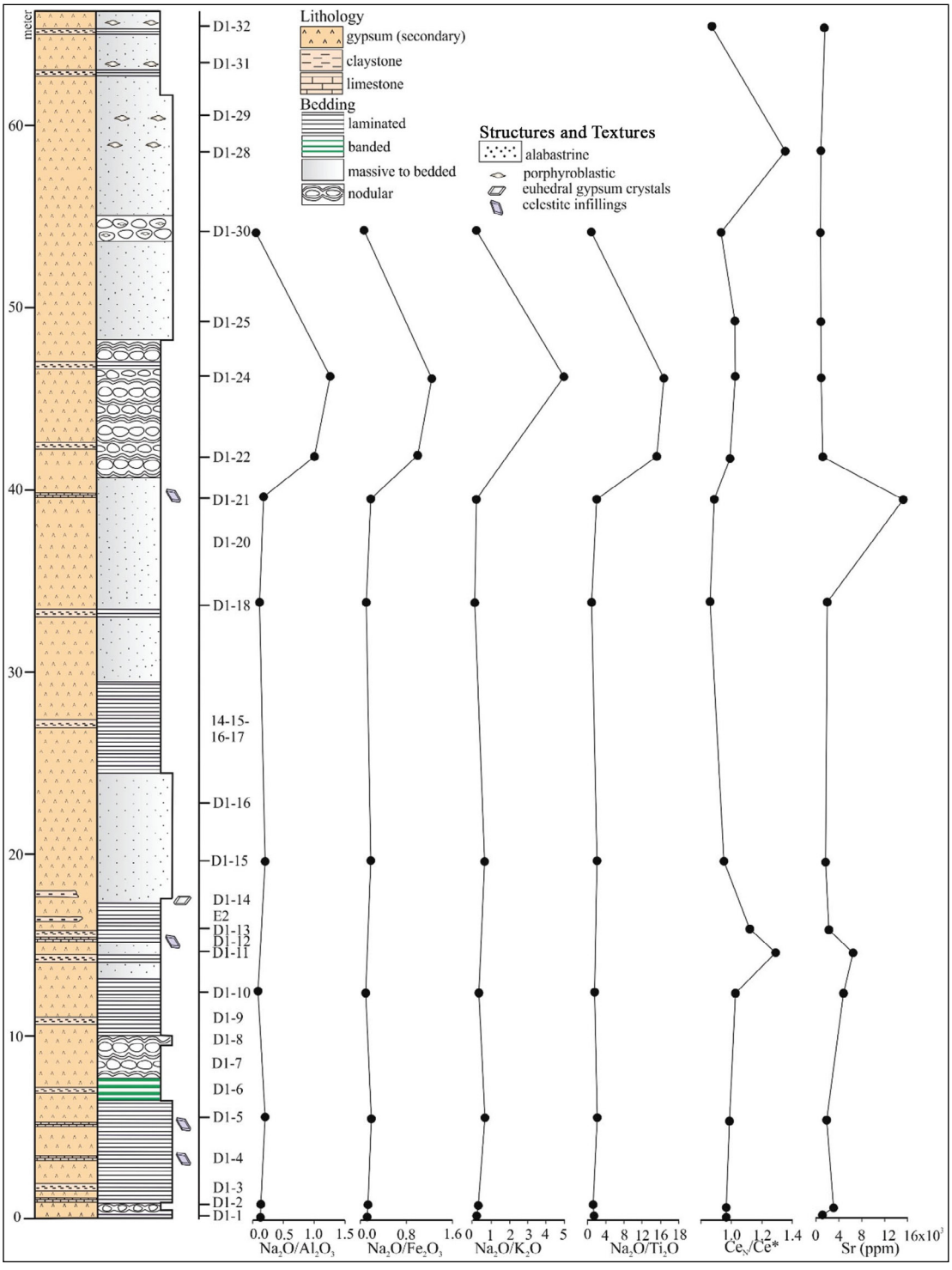

Figure 7- Chemostratigraphic characteristics of the Aşkale evaporites in the Pırnakapan section.

to evaporitic fluids in the paleo - environment of deposition, or else may indicate that seawater was very shallow during evaporite formation; in other words, in an area close to land rather than in the open sea (Bahadori et al., 2011). Additionally, it is noteworthy that despite textural differences in the Aşkale evaporites and the greater abundance of anhydrite, the above - mentioned oxide ratios do not show significant variations (Figure 7). Similarly, Sr contents are significantly higher in stratigraphic horizons with carbonate precipitation, clastic material input, and / or those associated with celestite precipitation.

5.3. Isotopic Characteristics

Sulfur isotope geochemistry and isotopic fractionation patterns can reveal valuable information about the sources of sulfur in a sediment, the mechanisms of sulfate reduction, and the kinetics of formation of sulfate minerals. The present - day seawater $\delta^{34}S$ composition is around 21 ‰ (Rees et al., 1978, Ohmoto, 1986), but this value lies somewhere between 10 ‰ and 30 ‰ for ancient marine evaporites (Garrels and Lerman, 1984).

In modern oceans, the $\delta^{34}S$ value of dissolved sulfate is 19.3 - 21.12 ‰ (Playà et al., 2007). When $\delta^{34}S$ fractionation between gypsum and water is below a mean value of 1.65 ‰ (Playà et al., 2007), fluids that could have formed the Aşkale gypsum and anhydrite would have had a mean $\delta^{34}S_{CDT}$ of 23.22 ‰, which matches normal marine values. While $\delta^{34}S$ ratios are not distinctive enough to be used to distinguish marine and non - marine evaporites in the geological record, the comparison of the frequency distribution of $\delta^{34}S_{CDT}$ values for marine and non - marine evaporites across Turkey (Palmer et al., 2004) with $\delta^{34}S_{CDT}$ values from the Aşkale evaporite samples (Figure 8) suggests that the latter resemble marine evaporites. When $\delta^{34}S_{CDT}$ values obtained from the Aşkale evaporites are compared with $\delta^{34}S$ values from Tertiary marine sulfates forming in other Messinian basins (Lu and Meyers, 2003; Playà et al., 2007; Tekin et al., 2010), they also appear to be similar. For example, the $\delta^{34}S$ values of marine sulfates in the İskenderun - Hatay (Turkey) basin are 20.7 - 25.1 ‰ (Tekin et al., 2010) and are 21.8 - 22.5 ‰ for those in the Gulf of Carpentaria, Australia, (Playà et al., 2007).

Figure 8 compares the frequency distribution of $\delta^{18}O$ values from marine and non - marine evaporites in Turkey (Palmer et al., 2004) with the frequency distribution of $\delta^{18}O$ values for the Aşkale evaporites. Though the Aşkale evaporites resemble both groups, they overlap with marine evaporites. The $\delta^{18}O$ values of sulfate - rich samples do not correlate well with age, as the $\delta^{18}O$ values of sulfate minerals in marine evaporites rise and fall during natural geological processes. For example, $\delta^{18}O$ values were ~17 ‰ in the Precambrian, ~10 ‰ in the Permian, ~16 ‰ in the Triassic, and ~12 - 13 ‰ in the Cenozoic period (Claypool et al., 1980). Considered together, the $\delta^{18}O$ isotopic composition of the Early - Miocene Aşkale evaporites is like that of marine evaporites.

The frequency distribution of Sr isotope values for marine (mean $\Delta_{SW} = -190.2$) and non - marine (mean $\Delta_{SW} = -92$) evaporites of Turkey (Palmer et al., 2004) are shown together with $^{87}Sr / ^{86}Sr$ distributions in Figure 8. Additionally, when the mean $^{87}Sr / ^{86}Sr$ found by Palmer et al. (2004) is considered, marine evaporites have $\Delta_{SW} = -190.2$ (n = 16) and non - marine evaporites have $\Delta_{SW} = -92$ (n = 21). It is not possible to say from these data that $^{87}Sr / ^{86}Sr$ ratios can effectively distinguish between marine and non - marine evaporites; however, the $^{87}Sr / ^{86}Sr$ ratios of the Aşkale evaporites ($\Delta_{SW} = -169.8$ to -99.9) are lower than those of Messinian seawater ($^{87}Sr / ^{86}Sr$ = 0.708825 - 0.708954 and $\Delta_{SW} = -34.8$ to -21.9; Burke et al., 1982; Müller and Mueller, 1991). The $^{87}Sr / ^{86}Sr$ ratio of modern seawater is much higher than the values for the Aşkale evaporites (0.709173 - 0.70920: Denison et al., 1998; Playà et al., 2007). As such, the Aşkale evaporite samples isotopically resemble Messinian seawater, but their lower $^{87}Sr / ^{86}Sr$ values emphasize that continental fluid input and variations in Sr isotopic composition were likely important during the accumulation of Ca - sulfate. The $\delta^{34}S_{CDT}$ and $\delta^{18}O$ isotope values measured in anhydrite and gypsum match those of marine environments, which have 21.3 - 25.62 ‰ and 11.5 - 19.1 ‰, respectively. Similar $^{87}Sr / ^{86}Sr$ and $\delta^{18}O$ values have been reported from other evaporitic basins by Müller (1962), Turekian (1964), Emery and Robinson (1992), Faure and Powell (1972), and Tekin (2001).

As sulfur isotopes cannot identify the source of evaporate - forming fluids, Sr isotopes should be used to provide more reliable constraints on the paleo - environmental conditions (Denison et al., 1998; Playà et al., 2000). On a plot of $\delta^{34}S_{CDT}$ against $^{87}Sr / ^{86}Sr$

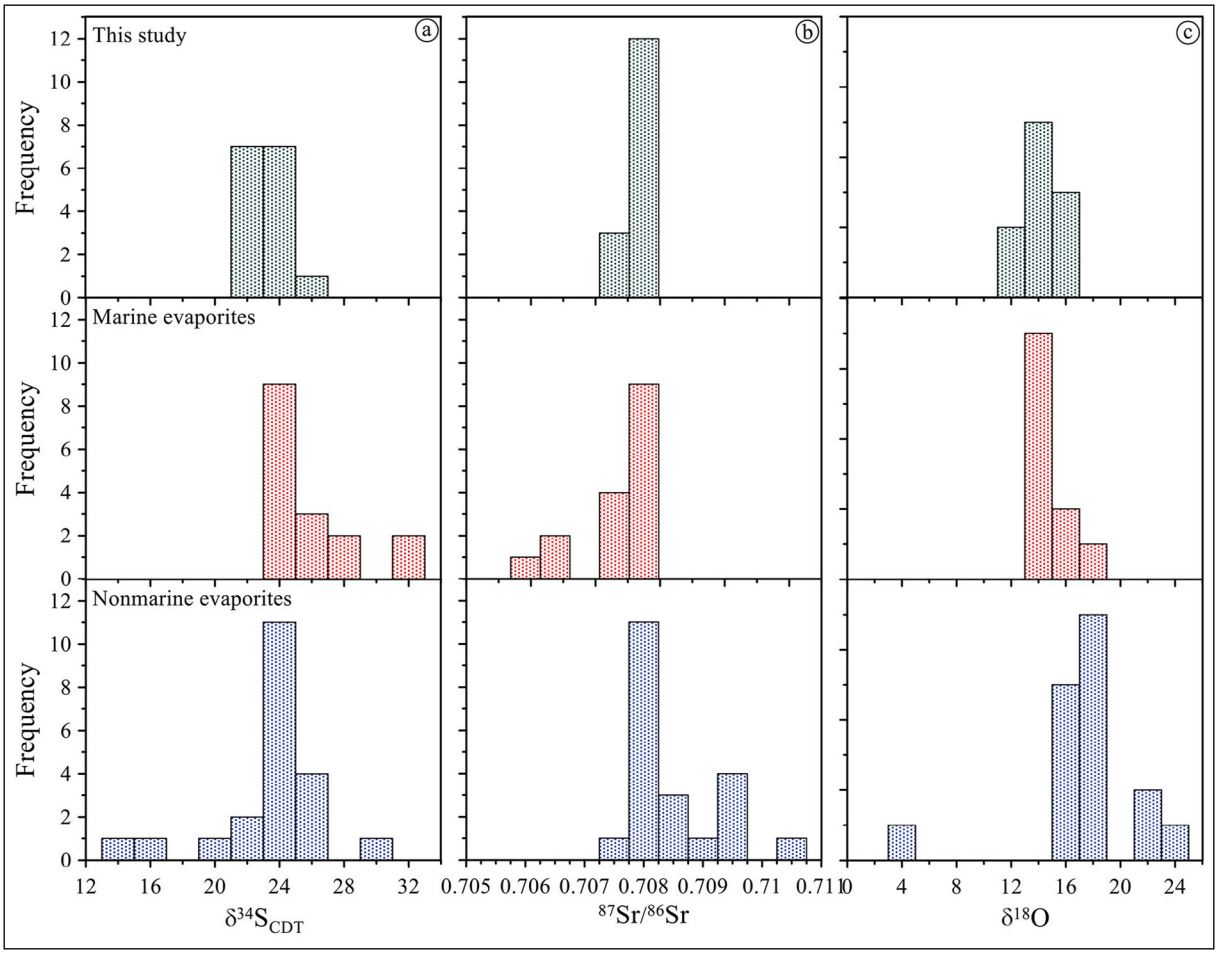

Figure 8- a - c) Histograms showing the distribution of $\delta^{34}S_{CDT}$, ^{87}Sr / ^{86}Sr, and $\delta^{18}O$ values in gypsum and anhydrite from the Aşkale evaporates, compared to those of non-marine and marine evaporites in Turkey (Palmer et al., 2004).

(Figure 9a), Aşkale evaporite samples (apart from nodular gypsum sample A1) have slightly higher ^{87}Sr / ^{86}Sr values than Cenozoic marine evaporites in Turkey. This may be due to the Aşkale evaporites forming in an isolated marine environment (salina: Denison et al., 1988), as shown by Sr isotope ratios, rather than in an open - marine environment, as accepted for the primary formation. On a plot of $\delta^{34}S_{CDT}$ against $\delta^{18}O$ (Figure 9b), the Aşkale gypsum and anhydrite samples have values that overlap with those of marine evaporites (Palmer et al., 2004). Additionally, the positive correlation between $\delta^{34}S_{CDT}$ and $\delta^{18}O$ for the Aşkale gypsum and anhydrite samples (Figure 9b) display similarities with those of sulfate samples precipitated in marine evaporative basins around Mediterranean region (Lu and Meyers, 2003). Obtained $\delta^{34}S_{CDT}$ and $\delta^{18}O$ values have a wide isotope ranges suggesting either a nonmarine contribution or an effective geochemical process to shift isotopic values. These geochemical processes were discussed in detail for the Upper Miocene evaporites from Spain by Lu and Meyers (2003) and summarized as redox reactions or reservoir effects in marine environment. In case of redox processes, dissolved sulfates undergo partial bacterial reduction to sulfides during or before gypsum precipitation and, $\delta^{34}S$ and $\delta^{18}O$ will have relatively higher values in the dissolved sulfate and lower values in sulfides due to preference of light isotopes by sulfate reducing bacteria (Mizutani and Rafter, 1969). Exposing to free oxygen, sulfide would be reoxidized to sulfate. Lu and Meyers (1997) indicate limitations of redox reactions but also imply that these cycling processes led to significantly elevated and variable $\delta^{34}S$ and $\delta^{18}O$. From this perspective, the elevated $\delta^{34}S_{CDT}$ and $\delta^{18}O$ values of the Aşkale gypsum and anhydrite samples may be caused by the reduction and oxidation reactions of sulfides.

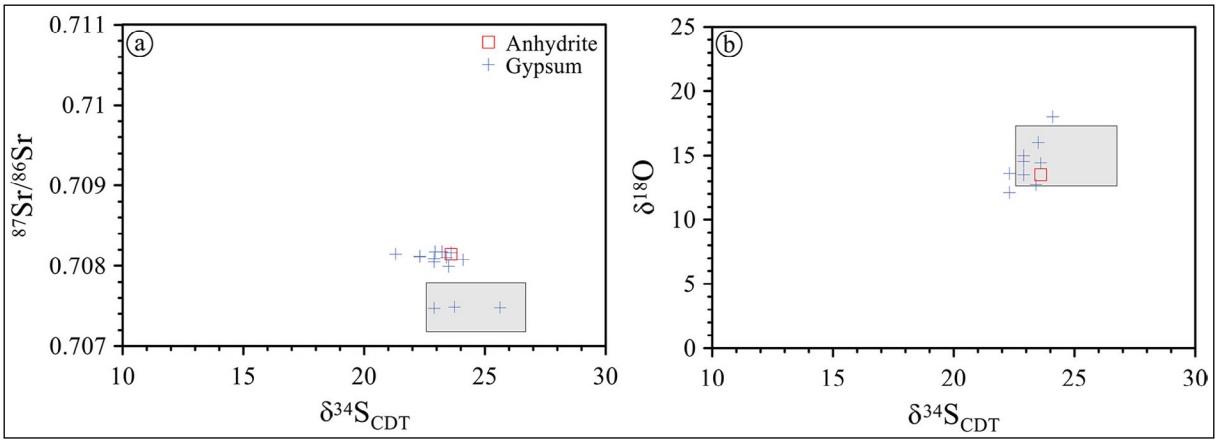

Figure 9- Plots of a) $\delta^{34}S_{CDT}$ versus ^{87}Sr / ^{86}Sr, and b) $\delta^{34}S_{CDT}$ versus $\delta^{18}O$ for the Aşkale evaporites. Gray field refers to gypsum and anhydrite compositions from the Cenozoic marine evaporites in Turkey (Palmer et al., 2004).

Assessing the seawater isotopic composition together with Sr and sulfur isotope results provides important information about the geological history of the Aşkale evaporite sequence. Secular variation in ^{87}Sr / ^{86}Sr and $\delta^{34}S$ (Paytan et al., 1998; McArthur et al., 2001) is shown in Figure 10, and stratigraphic data thus constrain the age of the Aşkale evaporites to be Early Miocene (Tarhan et al., 1992). Based on this interpretation, the mean age for Sr and sulfur isotope data is 19.5 Ma, which lies within the Lower Miocene. As anhydrite ^{87}Sr / ^{86}Sr values do not vary as a result of deformation and recrystallization (Dejonghe et al., 1998), the seawater isotopic composition can be interpreted to have been similar (albeit slightly higher) during deposition of the Aşkale evaporite samples (Figure 10). Additionally, Sr, S, and O isotopic values of the Aşkale evaporites imply formation in a typical marine environment, as $\delta^{34}S$ and $\delta^{18}O$ values for sulfate minerals precipitating from seawater today are around 20.0 ‰ and 9.50 ‰ (Longinelli, 1989), respectively. Fractionation factors associated with precipitation (1.65 ‰ for S and 3.5 ‰ for O: Lloyd, 1968; Thode and Monster, 1965; Céndon et al., 2004) account for this small difference between predicted and measured values. The similarity of isotopic values within the basin show that the Aşkale evaporites are entirely of marine origin, and match values reported for marine evaporites by Claypool et al. (1980).

6. Conclusions

1) Whole - rock major - , trace - , and rare earth - element contents, and ^{87}Sr / ^{86}Sr, $\delta^{34}S$ and $\delta^{18}O$ isotopic data were determined for a suite of Aşkale evaporites. These data reveal that evaporites from different lithofacies show some input of continental

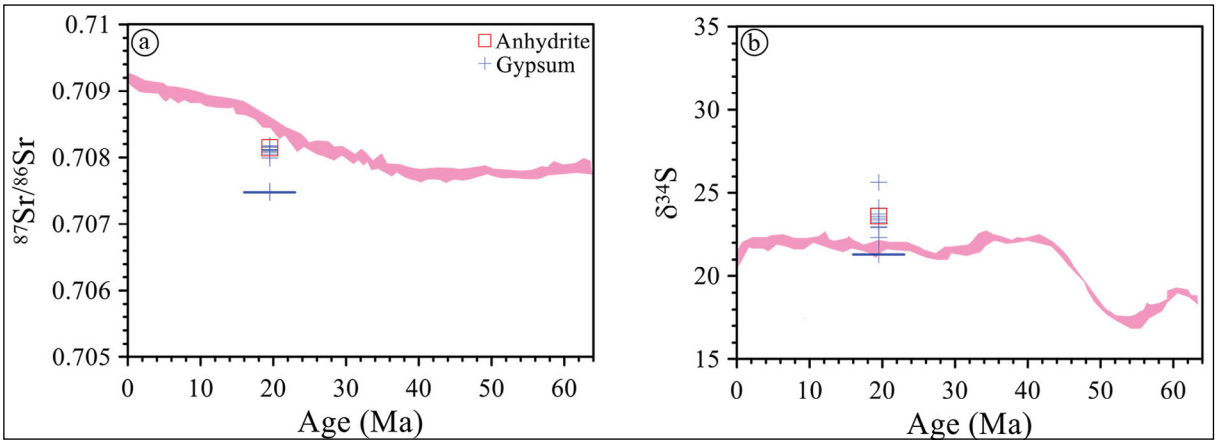

Figure 10- Plots of age (Ma) versus a) ^{87}Sr / ^{86}Sr and b) $\delta^{34}S$ for the Aşkale evaporites. Shaded fields indicate seawater ^{87}Sr / ^{86}Sr (McArthur, 2001) and $\delta^{34}S$ (Paytan et al., 1998) compositions.

detritic material, as indicated by enrichments in light REEs, variable Ce / Ce* ratios, and Ni, Cu, Co, Fe, and Mg contents.

2) In the Aşkale evaporites, strong negative and positive Eu anomalies that are independent of lithofacies transitions in these evaporites record periods of deepening and shallowing of the paleo - environment of deposition, linked to climatic and tectonic activity and the presence of occasional freshwater input. The Sr content of evaporites indicates the importance of marine - sourced Sr; however, especially high Sr contents are associated with the formation of epigenetic celestite and minor volcanic input.

3) ^{87}Sr / ^{86}Sr isotopic ratios, and $\delta^{34}S_{CDT}$ and $\delta^{18}O$ values for the Aşkale gypsum - and anhydrite - samples indicate that these evaporites formed in a marine environment.

4) Examination of the geochemical characteristics of the Aşkale evaporites according to stratigraphic height and vertical lithofacies variations shows that they developed in subtropical conditions, most likely in a shallow platform or lagoonal environment that experienced multiple transgressions.

Acknowledgments

This study was funded by the Turkish Scientific Research Council (TÜBİTAK - ÇAYDAG project no: 110Y023). The authors are grateful to the editor in chief H. Mutlu, reviwers Z.S. Karakaş and O. Ersoy for their constructive comments to improve the paper.

References

Abdioğlu, E., Arslan, M., Gündoğan, İ., Helvacı, C. 2013. Aşkale (Erzurum) Civarındaki Evaporitlerin Mineralojik, Jeokimyasal ve İzotopik Özellikleri, KD Türkiye. TÜBİTAK Projesi, Proje no: 110Y023.

Abdioğlu, E., Arslan, M., Aydınçakır, D., Gündoğan, İ., Helvacı, C. 2015. Stratigraphy, mineralogy and depositional environment of the evaporite unit in the Aşkale (Erzurum) sub - basin, Eastern Anatolia (Turkey). Journal of African Earth Sciences 111, 100-112.

Adabi, M. H. 2004. Sedimentary Geochemistry. Arianzamin Publication, Iran.

Alptekin, Ö. 1973. Focal Mechanism of Earthquakes in Western Turkey and Their Tectonic Implications. PhD Thesis, New Mexico Institute of Mining and Technology, Socorro, USA.

Aydınçakır, D. 2013. Pırnakapan (Aşkale, Erzurum) civarındaki evaporitlerin mineralojik, petrografik ve jeokimyasal incelenmesi. Karadeniz Teknik Üniversitesi, Fen Bilimleri Enstitüsü, Yüksek Lisans Tezi.

Bahadori, A., Carranza, E. J. M., Soleimani, B. 2011. Geochemical analysis of evaporite sedimentation in Gachsaran Formation, Zeloi oil field, southwest Iran. Journal of Geochemical Exploration 111, 97-112.

Baysal, O., Ataman, G. 1980. Sedimentology, mineralogy and geochemistry of a sulphate series (Sivas - Turkey). Sedimentary Geology 25, 67-81.

Brinkmann, R. 1976. Geology of Turkey. Elsevier, Amsterdam.

Burke, W. H., Denison, R. E., Hetherington, E. A., Koepnik, R. B., Nelson, H. F., Otto, J. B. 1982. Variation of seawater ^{87}Sr / ^{86}Sr throughout Phanerozoic time. Geology 10, 516-519.

Cendón, D. I., Chivas, A. R., García, A. 2004. Chemistry of the rivers in the Gulf of Carpentaria drainage division and possible correlations with the sedimentary record during lake phases. 17th Australian Geological Convention. Dynamic Earth: Past, Present and Future. Hobart, Australia, 73, 228.

Claypool, G. E., Holser, W. T., Kaplan, I. R., Sakai, H., Zak, I. 1980. The age curves of sulfur and oxygen isotopes in marine sulfate and their mutual interpretation. Chemical Geology 28, 199-260.

Crockford, P. W., Kunzmann, M., Bekker, A., Hayles, J., Bao, H., Halverson, G. P., Peng, Y., Bui, T. H., Cox, G. M., Gibson, T. M., Wörndle, S., Rainbird, R., Lepland, A., Swanson - Hysell, N. L., Master, S., Sreenivas, B., Kuznetsov, A., Krupenik, V., Wing, B. A. 2019. Claypool continued: Extending the isotopic record of sedimentary sulfate. Chemical Geology 513, 200-225.

Çiner, A., Koşun, E., Deynoux, M. 2002. Fluvial, evaporitic and shallow-marine facies architecture, depositional evolution and cyclicity in the Sivas Basin (Lower to Middle Miocene), Central Turkey. Journal of Asian Earth Sciences 21, 147-165.

Dejonghe, L., Demaiffe, D., Weis, D. 1998. Strontium isotope geochemistry of anhydrites and calcite pseudomorphs after anhydrite from Paleozoic

formations in Belgium. Chemical Geology 144, 63-71.

Denison, R. E., Kırkland, D. W., Ewans, R. 1998. Using strontium isotopes to determine the age and origin of anhydrite and gypsum beds. The Journal of Geology 106, 1-7.

Emelyanov, E. M., Shimkus, K. M. 1986. Geochemistry and Sedimentology of the Mediterranean Sea. Springer, Paris.

Emery, D., Robinson, A. 1992. Inorganic Geochemistry Applications to Petroleum Geology. Blackwell Scientific Publications, Oxford.

Faure, G., Powell, J. L. 1972. Strontium Isotope Geology. Springer-Verlag, New York.

Gallet, S., Jahn, B. M., Torii, M. 1996. Geochemical characterization of the Luochuan loesspaleosol sequence, China, and paleoclimatic implications. Chemical Geology 133, 67-88.

Garrels, R. M., Lerman, A. 1984. Coupling of the sedimentary sulfur and carbon cycles; an improved model. American Journal of Science 284, 989-1007.

Gökçe, A., Ceyhan, F. 1988. Sivas güneydoğusundaki Miyosen yaşlı jipsli çökellerin stratigrafisi, yapısal özellikleri ve oluşumu. Cumhuriyet Earth Science Journal 5, 1, 91-113 (in Turkish).

Gündoğan, İ. 2000. Geology, Mineralogy-Petrography and Economic Potential of the Upper Miocene Evaporites in The Beypazarı and Çankırı - Çorum Basins. PhD Thesis, The Graduate School of Natural and Applied Sciences, DEU.

Gündoğan, İ., Önal, M., Depçi, T. 2005. Sedimentology, petrography and diagenesis of Eocene - Oligocene evaporites: the Tuzhisar Formation, SW Sivas Basin, Turkey. Journal of Asian Earth Sciences 25, 791-803.

Gündoğan, İ., Helvacı, C., Sözbilir, H. 2008. Gypsiferious carbonates at Honaz Dağı (Denizli): First documentation of Triassic gypsum in western Turkey and its tectonic significance. Journal of Asian Earth Sciences 32, 49-65.

Hasselöv, M., Lyvén, D., Haraldsson, C., Sirinawin, W. 1999. Determation of continous size and trace element distribution of field-flow fractionation with ICPMS. Analytical Chemistry 71, 3497-3502.

Helvacı, C. Yağmurlu, F. 1995. Geological setting and economic potential of the lignite and evaporite-bearing Neogene basins of Western Anatolia, Turkey. Israel Journal of Earth Sciences 44, 91-105.

Horner, T. J., Pryer, H. V., Nielsen, S. G., Crockford, P. W., Gauglitz, J. M., Wing, B. A., Ricketts, R. D. 2017. Pelagic barite precipitation at micromolar ambient sulfate, Nature Communications 8, Article number: 1342.

Kamber, B. S., Greig, A., Collerson, K. D. 2005. A new estimate for the composition of weathered young upper contitnental crust from alluvial sediments, Queensland, Australia. Geochimica et Cosmochimica Acta 69, 4, 1041-1058.

Kasprzyk, A. 2003. Sedimentological and diagenetic patterns of anhydrite deposits in the Badenian evaporite basin of the Carpathian Foredeep, southern Poland. Sedimentary Geology 158, 167-194.

Keskin, M. 2003. Magma generation by slab steepening and breakoff beneath a subduction-accretion complex: An alternative model for collision-related volcanism in Eastern Anatolia, Turkey. Geophysical Research Letters 30, 24, 1-4.

Ketin, İ. 1966. Tectonic units of Anatolia (Asia Minor). Bulletin of the Mineral Research and Exploration 66, 23-34.

Kornexl, B. E., Gehre, M., Höfling, R., Werner, R. A. 1999. On-line $\delta^{18}O$ Measurement of organic and inorganic substances. Rapid Communications in Mass Spectrometry 13, 1685-1693.

Krauskopf, K. B. 1979. Introduction to Geochemistry. McGraw-Hill Book Company, New York.

Kushnir, J. 1980. The coprecipitation of strontium, magnesium, sodium, potassium, and chloride ions with gypsum: an experimental study. Geochimica et Cosmochimica Acta 44, 1471-1482.

Kushnir, J. 1982. The partitioning of seawater cations during the transformation of gypsum to anhydrite. Geochimica et Cosmochimica Acta 46, 433-446.

Lloyd, R. M. 1968. Oxygen isotope behavior in the sulphate-water system. Journal of Geophysical Research 73, 6099-6110.

Longinelli, A. 1989. Oxygen-18 and sulphur-34 in dissolved oceanic sulphate and phospate. In: Fritz, P., Fontes, J.C. (Eds.), Handbook of Environmental Isotope Geochemistry. The Marine environment. Elseiver, Amsterdam, 219-255.

Lu, F. H., Meyers, W. J. 1997. Sr, S, O_{SO4} isotopes and quantitative models of Messinian gypsum, the Nijar Basin, Spain (Abstract). International Applied Isotope Geochemistry (AIG-2) Conference, Calgary.

Lu, F. H., Meyers, W.J. 2003. ^{87}Sr / ^{86}Sr, $\delta^{34}S$ and $\delta^{18}O$ (SO_4) isotopes of Messinian evaporites, modeling and environmental significance. Journal of Sedimentary Research 73, 443-449.

Ludden, J. N., Thompson, G. 1979. An evaluation of the behaviour of the REE elements during the weathering of seafloor basalt. Earth and Planetary Science Letters, 43, 85-92.

Mason, B., Moore, C. B. 1982. Principles of Geochemistry. Wiley, New York.

McArthur, J. M., Howarth, R. J., Bailey, T. R. 2001. Strontium isotope stratigraphy: LOWESS version 3: best fit to the marine Sr - isotope curve for 0 - 509 Ma and accompanying look-up table for deriving numerical age. The Journal of Geology 109, 155-170.

McKenzi, D. P. 1976. The East Anatolian Fault: a major structure in Eastern Turkey. Earth and Planetary Science Letters 29, 189-193.

Menzies, M., Seyfried, W., Blanchard, D. 1979. Experimental evidence of rare earth element immobility in Greenstones. Nature 282, 398-399.

Mizutani, Y., Rafter, T.A. 1969. Oxygen isotopic composition of sulfates, 4. Bacterial fractionation of oxygen isotopes in the reduction of sulphate and in the oxidation of sulphur: New Zealand. Journal of Science, 12, 60-68.

Müller, D. W., Mueller, P.A. 1991. Origin and age of the Mediterranean Messinian evaporites; implications from Sr isotopes. Earth and Planetary Science Letters 107, 1-12.

Müller, G. 1962. Zur Geochemie des Strontiums in Ozeanen evaporites unter besonderer Berücksichtigung der sedimentaren Coelestin lagerstatte von Hemmelte-West (Süd Oldenburg). Geologie 11, 1-90.

Nesbitt, H. W., Young, G. M. 1982. Early Proterozoic climates and plate motions inferred from major element chemistry of lutites. Nature 299, 715-717.

Ohmoto, H. 1986. Stable isotope geochemistry of ore deposits. In: Valley, J. W., Taylor J.R., H.P., O'Neil, J.R. (Eds.), Stable Isotopes in High Temperature Geological Processes. Reviews in Mineralogy, Mineralogical Society of America, 16, 491-560.

Okay, A. I., Tüysüz, O. 1999. Tethyan sutures of northern Turkey. In: Durand, B., Jolivet, L., Horváth, F., Séranne M. (Eds.), The Mediterranean Basins: Tertiary Extension within the Alpine Orogen. Geological Society, London, Special Publications 156, 475-515.

Ortí, F., Rosell, L. 2000. Evaporative systems and diagenetic patterns in the Calatayud Basin (Miocene, central Spain). Sedimentology 47, 665-685.

Ortí, F., Gündoğan, İ., Helvacı, C. 2002. Sodium sulphate deposit of Neogene age: the Kirmir Formation, Beypazarı Basin, Turkey. Sedimentary Geology 146, 305-333.

Ortí, F., Rosell, L., Ingles, M., Playà, E. 2007. Depositional models of lacustrine evaporates in the SE margin of the Ebro Basin (Paleogene) NE Spain. Geologica Acta 5, 19-34.

Palmer, M. R., Helvacı, C., Fallick, A. E. 2004. Sulphur, sulphate, oxygen and strontium isotope composition of Cenozoic Turkish evaporates. Chemical Geology 209, 341-356.

Pandarinath, K., Prasad, S., Gupta, S. K. 1999. A 75 ka record of palaeoclimatic changes inferred from crystallinity of illite from Nal Sarovar, Western India. Journal of the Geological Society of India 54, 515-522.

Paytan, A., Kastner, M., Campbell, D., Thiemens, M.H. 1998. Sulphur isotopic composition of Cenozoic seawater sulphate. Science 282, 1459-1462.

Playà, E., Ortí, F., Rosell, L. 2000. Marine to non-marine sedimentation in the Upper Miocene evaporites of the Eastern Betics, SE Spain: sedimentological and geochemical evidence. Sedimentary Geology 133, 135-1666.

Playà, E., Cendon, D. I., Trave, A., Chivas, A. R., Garcia, A. 2007. Using multiple geochemical proxies to trace origin of gypsum (Gulf of Carpentaria, Australia, -70ka). Geogaceta 42, 135-138.

Rees, C. E., Jekins, W.E., Monster, J. 1978. The sulphur isotopic composition of ocean water sulphate. Geochimica et Cosmochimica Acta 42, 377-381.

Rosell, L., Orti, F., Kasprzyk, A., Playa, E., Peryt, T. M. 1998. Strontium geochemistry of Miocene primary gypsum; Messinian of southeastern Spain and Sicily and Badenian of Poland. Journal of Sedimentary Research 68, 63-79.

Roy, P. D., Smykatz-Kloss, W., Sinha, R. 2006. Late Holocene geochemical history inferred from Sambhar and Didwana playa sediments, Thar Desert, India: comparison and synthesis. Quaternary International 144, 84-98.

Roy, P. D., Nagar, Y. C., Juyal, N., Smykatz-Kloss, W., Singhvi, A. K. 2009. Geochemical signatures of Late Holocene paleo - hydrological changes from Phulera and Pokharan saline playas near the eastern and western margins of the Thar Desert,

India. Journal of Asian Earth Sciences 34, 275 - 286.

Rushdi, A. I., McManus, J., Collier, R. W. 2000. Marine barite and celestite saturation in seawater. Marine Chemistry 69, 19-31.

Sancay, R. E. 2005. Palynostratigraphic and Palynofacies Investigation of the Oligocene - Miocene Units in the Kars - Erzurum - Muş Sub-Basins (Eastern Anatolia). PhD Thesis, Middle East Technical University.

Smykatz-Kloss, W., Roy, P. D. 2010. Evaporite mineralogy and major element geochemistry as tools for paleoclimatic investigations in arid regions: a synthesis. Boletin De La Sociedad Geológica Mexicana 62, 3, 379-390.

Sungurlu, O. 1971. İ45a, İ45b, İ46a, İ46b, İ47a, İ47b, paftalarına ait 1 / 50000'lik jeoloji haritaları. TPAO, Ankara.

Sverjensky, D. A. 1984. Europium Redox Equilibria in Aqueous Solution. Earth and Planetary Science Letters 67, 70-78.

Şahintürk, Ö. 1992. Tercan - Çayırlı Basenleri'nin jeolojisi ve hidrokarbon olanakları, TPAO Arama Grubu Rap. No. 3070, Ankara (in Turkish, unpublished).

Şahintürk, Ö., Kasar, S. 1980. Tercan - Çayırlı Baseninin Jeolojisi ve Hidrokarbon Olanakları (Geology and Hydrocarbon Potential of the Tercan-Çayırlı Basin). TPAO Arama Grubu Raporu, no. 1446 (in Turkish, unpublished).

Şahintürk, Ö., Şaroğlu, F., Çaptuğ, A., Temel, Ö., İlleez, H. İ., Tekin, T. 1997. Ağrı Yöresinin Jeolojisi ve Hidrokarbon Olanakları (Geology and Hydrocarbon Potential of the Ağrı Area). TPAO Arama Grubu Rapor No. 3790, Ankara (in Turkish, unpublished).

Şengör, A .M. C. 1980. Türkiye'nin Neotektoniğinin Esasları (Fundamentals of the Neotectonics of Turkey). Publication of Geological Society of Turkey, 2, Ankara (in Turkish).

Şengör, A. M. C., Özeren, S., Zor, E., Genç, T. 2003. East Anatolian high plateau as a mantle-supported, N-S shortened domal structure. Geophysical Research Letters 30, 8044.

Tarhan, N., Deveciler, E., Karabalık, N. N., Akdoğan, E., Çolak, T., Kar, H. 1992. Aşkale - Çat (Erzurum) Dolayının Jeolojisi (Geology of the Aşkale - Çat (Erzurum) area). Maden Tetkik ve Arama Genel Müdürlüğü, Ankara (in Turkish, unpublished).

Tchalenko, J. S. 1977. A reconnaissance of the seismicity and tectonics of the northern border of the Arabian plate (Lake Van Region). Revule de Geographie Physique et de Geologie Dynamiqu 19, 2, 189-208.

Tekin, E. 2001. Stratigraphy, Geochemistry and Depositional Environment of the Celestine - bearing gypsiferous Formations of the Tertiary Ulaş - Sivas Basin, East - Central Anatolia (Turkey). Turkish Journal of Earth Sciences 10, 35-49.

Tekin, E., Varol, B., Ayyıldız, T. 2010. Sedimentology and paleoenvironmental evolution of Messinian evaporates in the İskenderun - Hatay basin complex, Southern Turkey. Sedimentary Geology 229, 4, 282-298.

Tekin, T., Alişan, C., Işık, U., Akça, N., Aras, M., Günal, B. 2000. Aşkale-1 Kuyusu Sonuç Raporu (The Aşkale-1 Final Well Report) TPAO Araştırma Grubu Rapor no: 2514, Ankara (in Turkish, unpublished).

Thode, H. G., Monster, J. 1965. Sulphur isotope geochemistry of petroleum, evaporites and ancient seas. In: Young, A., Galley, J.E. (Ed.), Fluids in Subsurface Environments. American Association of Petroleum Geologists, Tulsa, Oklahoma, USA, 4, 367-377.

Toulkeridis, T., Podwojewski, P., Clauer, N. 1998. Tracing the source of gypsum in New Caledonian soils by REE contents and S - Sr isotopic compositions. Chemical Geology 145, 61-71.

Turekian, K. K. 1964. The marine geochemistry of strontium. Geochimica et Cosmochimica Acta 28, 1479-1496.

Türkmen, İ. 2004. Facies and evaporite genesis of the Kuşçular Formation (Lower Paleocene) saline playa complex, Eastern Turkey. Journal of Asian Earth Science 24, 91-104.

Ueda, A., Krouse, H.R. 1986. Direct Conversion of Sulphide and Sulphate Minerals to SO_2 for Isotope Analysis. Geochemical Journal 20, 209-212.

Usdowski, E. 1967. Der Einbau von Sr in Gips und Anhydrit. Ann. Meet. Deutsche Mineral. Gesell., Berlin.

Warren, J. K. 2010. Evaporites through time: Tectonic, climatic and eustatic controls in marine and nonmarine deposits. Earth Science Reviews 98, 217-268.

Warren, J. K., Kendall, C.G.St.C. 1985. Comparison of marine sabkhas (subaerial) and salina (subaqueous) evaporites: modern and ancient. AAPG Bulletin 69, 1013-1023.

Yeşilova, Ç., Helvacı, C., Carrillo, E. 2018. Evaporitic sedimentation in the Southeastern Anatolian

Foreland Basin: New insights on the Neotethys closure. Sedimentary Geology 369, 13-27.

Yılmaz, Y. 1993. New evidence and model on the evaluation of the southeast Anatolian orogen. Geological Society of America Bulletin 105, 251-271.

Zeybek, B. 2007. Geochemical Studies of Porsuk Formation (Pliocene) Evaporites, Middle Sakarya Region, Central Anatolia, Turkey. MSc thesis, The Graduate School of Natural and Applied Sciences, Ankara University (in Turkish).

Supplementary Table 1- Major (wt%) and trace element (ppm) compositions of the Aşkale evaporites.

	D1-1	D1-2	D1-5	D1-10	D1-11	D1-13	D1-15	D1-18	D1-25	D1-28	D1-30	D1-22	D1-24	D1-21
	The Pırnakapan Section													
	gypsum-rich samples											*anhydrite-rich samples*		*limestone*
SiO_2 wt. %	2.23	1.52	0.81	0.88	0.21	0.43	1.78	1.56	0.05	0.03	1.55	0.13	0.18	2.38
Al_2O_3	0.56	0.36	0.18	0.11	0.03	0.04	0.19	0.37	0.01	< 0.01	0.28	0.03	0.06	0.62
$Fe_2O_3^*$	0.25	0.18	0.1	0.12	0.02	0.04	0.11	0.18	0.02	0.01	0.17	0.03	0.04	0.28
MnO	0.004	0.003	0.002	0.008	0.002	0.002	0.004	0.006	0.002	0.002	0.007	0.002	0.003	0.009
MgO	0.36	0.34	0.21	2.55	0.09	0.04	1.38	1.05	0.02	0.04	0.36	0.03	0.05	0.59
CaO	30.92	30.69	31.99	29.8	31.99	32.3	30.42	30.06	32.98	32.68	32.25	41.85	40.23	48.14
Na_2O	0.03	0.02	0.02	0.01	< 0.01	< 0.01	0.02	0.02	< 0.01	< 0.01	0.01	0.03	0.05	0.05
K_2O	0.19	0.1	0.03	0.03	< 0.01	< 0.01	0.03	0.17	< 0.01	< 0.01	0.07	< 0.01	0.01	0.29
TiO_2	0.029	0.019	0.009	0.006	0.002	0.002	0.009	0.019	< 0.001	< 0.001	0.013	0.002	0.003	0.025
P_2O_5	< 0.01	0.01	< 0.01	< 0.01	< 0.01	< 0.01	< 0.01	0.01	< 0.01	< 0.01	< 0.01	0.02	0.02	0.04
LOI	21.82	21.48	21.38	22.82	20.81	20.93	21.56	21.85	20.99	20.76	21.24	3.65	3.38	39.01
Total	56.39	54.73	54.74	56.34	53.18	53.8	55.51	55.29	54.07	53.54	55.97	45.78	44.03	91.43
Cl wt. %	< 0.01	< 0.01	0.01	0.04	< 0.01	< 0.01	< 0.01	< 0.01	< 0.01	< 0.01	< 0.01	0.03	0.03	< 0.01
CO_2	0.37	0.25	0.22	3.64	0.09	0.18	1.52	1.04	0.07	0.14	0.79	0.06	0.28	38.6
SO_4	59.4	60	60.6	56.9	61.7	60.8	58.6	59.5	61	61.8	59.3	75.5	73.6	6.1
Br ppm	< 0.5	< 0.5	< 0.5	1.6	< 0.5	< 0.5	< 0.5	< 0.5	< 0.5	< 0.5	< 0.5	1.5	2.4	< 0.5
B	14.5	9.4	2.4	5.5	3.4	3.7	15	20.3	1.8	4.9	3.1	8.2	17.7	13.8
V	13	11	9	10	7	8	10	10	7	7	9	8	6	17
Ba	16	32	12	47	16	9	49	20	1	1	11	< 1	< 1	91
Sr	1312	2978	1911	4849	6464	2238	1681	1928	806	865	909	1197	1023	15150
Y	0.8	0.7	< 0.5	< 0.5	< 0.5	< 0.5	< 0.5	0.6	< 0.5	< 0.5	< 0.5	< 0.5	< 0.5	1.3
Zr	4.1	3.3	0.9	0.5	1.5	< 0.1	5.8	2.4	< 0.1	< 0.1	1.9	0.4	0.3	4.2
Ga	< 1	< 1	< 1	< 1	< 1	< 1	< 1	< 1	< 1	< 1	< 1	< 1	< 1	< 1
Ge	< 0.5	< 0.5	< 0.5	< 0.5	< 0.5	< 0.5	< 0.5	< 0.5	< 0.5	< 0.5	< 0.5	< 0.5	< 0.5	< 0.5
As	1.7	1	1.6	1.3	0.4	0.5	1.6	1.8	1.2	0.6	1.1	4.9	1.4	2.3
Rb	2.4	1.3	0.2	< 0.1	< 0.1	< 0.1	0.6	1.3	< 0.1	< 0.1	1	0.3	0.2	3.5
Nb	0.8	0.58	0.19	0.11	< 0.01	0.04	0.23	0.21	< 0.01	< 0.01	< 0.01	< 0.01	< 0.01	0.29
Mo	< 2	< 2	< 2	3	< 2	< 2	< 2	< 2	< 2	< 2	< 2	< 2	< 2	< 2
Ag	< 0.002	0.009	< 0.002	0.004	< 0.002	< 0.002	0.003	< 0.002	0.032	0.009	0.012	0.098	0.02	0.004
In	< 0.1	< 0.1	< 0.1	< 0.1	< 0.1	< 0.1	< 0.1	< 0.1	< 0.1	< 0.1	< 0.1	< 0.1	< 0.1	< 0.1
Sn	< 1	< 1	< 1	< 1	< 1	< 1	< 1	< 1	< 1	< 1	< 1	< 1	< 1	< 1
Sb	< 0.2	< 0.2	< 0.2	< 0.2	< 0.2	< 0.2	< 0.2	< 0.2	< 0.2	< 0.2	< 0.2	< 0.2	< 0.2	< 0.2
Cs	< 0.1	< 0.1	< 0.1	< 0.1	< 0.1	< 0.1	< 0.1	< 0.1	< 0.1	< 0.1	< 0.1	< 0.1	< 0.1	0.3
Hf	0.1	< 0.1	< 0.1	< 0.1	< 0.1	< 0.1	< 0.1	< 0.1	< 0.1	< 0.1	< 0.1	< 0.1	< 0.1	< 0.1
Ta	< 0.01	< 0.01	< 0.01	< 0.01	0.02	< 0.01	< 0.01	< 0.01	< 0.01	< 0.01	< 0.01	< 0.01	< 0.01	0.03
W	< 0.5	< 0.5	< 0.5	< 0.5	< 0.5	< 0.5	< 0.5	< 0.5	< 0.5	< 0.5	< 0.5	< 0.5	< 0.5	< 0.5
Tl	< 0.05	< 0.05	< 0.05	< 0.05	< 0.05	< 0.05	< 0.05	< 0.05	< 0.05	< 0.05	< 0.05	< 0.05	< 0.05	< 0.05
Pb	0.63	0.21	0.1	0.17	0.05	0.04	0.44	0.3	0.06	0.04	0.26	0.11	0.05	0.78
Bi	< 0.1	0.2	< 0.1	< 0.1	< 0.1	< 0.1	< 0.1	< 0.1	< 0.1	< 0.1	< 0.1	< 0.1	< 0.1	< 0.1
Th	0.22	0.17	0.06	0.06	0.04	< 0.01	0.1	0.15	< 0.01	< 0.01	0.11	0.06	0.08	0.3
U	0.163	0.183	0.123	0.254	0.095	0.043	0.084	0.225	< 0.005	< 0.005	0.101	0.045	0.058	2.57
Cd	< 0.01	< 0.01	0.01	0.02	< 0.01	< 0.01	0.02	0.01	< 0.01	0.01	< 0.01	< 0.01	< 0.01	0.05
Cr	< 20	< 20	< 20	< 20	< 20	< 20	< 20	< 20	< 20	< 20	< 20	< 20	< 20	< 20
Co	0.8	0.5	0.5	0.7	0.1	0.3	0.6	0.8	0.1	0.1	0.6	0.1	0.1	1.3
Ni	8.9	4.8	4.8	6.8	2.2	3	6.7	8	2.1	1.9	5	1.7	1.5	11.1
Cu	2.08	2.08	1.23	2.26	0.66	1.16	1.33	1.74	3.24	0.54	1.8	0.93	0.56	2.67
Zn	3.5	2.3	1.4	1.7	1	2.9	2	1.8	2.4	1.5	3	1.8	0.9	3.1

Supplementary Table 1- continue.

	D1-32	D2-4	D3-1	D3-2	D3-5	D3-4	D3-6	28	D2-2	K-22	K-25	K-24
	The Pırnakapan Section									The Kemerkaya Section		
	gypsum-rich samples								*claystone*	*gypsum-rich samples*		
SiO_2 wt. %	0.12	0.16	3.92	2	1.54	1.15	0.8	1.81	30.34	0.2	0.05	0.14
Al_2O_3	0.03	0.04	0.94	0.22	0.08	0.02	0.15	0.4	8.99	0.04	< 0.01	0.03
$Fe_2O_3^*$	0.04	0.03	0.42	0.13	0.05	0.02	0.09	0.19	4.85	0.03	0.03	0.02
MnO	0.004	0.003	0.007	0.005	0.002	0.002	0.004	0.003	0.077	0.002	0.002	0.002
MgO	0.02	0.02	1.18	1.7	0.18	0.08	0.28	0.46	2.66	0.04	< 0.01	0.03
CaO	32.39	32.1	30.2	30.98	32.29	32.92	33.13	30.35	21.57	32.52	32.59	32.19
Na_2O	< 0.01	< 0.01	0.13	0.02	0.01	< 0.01	0.01	0.02	0.63	< 0.01	< 0.01	< 0.01
K_2O	< 0.01	< 0.01	0.16	0.04	0.02	< 0.01	0.03	0.08	1.39	< 0.01	< 0.01	< 0.01
TiO_2	0.002	0.002	0.047	0.011	0.004	< 0.001	0.009	0.021	0.493	0.002	< 0.001	0.002
P_2O_5	0.03	< 0.01	0.02	< 0.01	0.02	0.04	0.03	< 0.01	0.09	< 0.01	< 0.01	< 0.01
LOI	20.94	20.66	22.69	21.76	21.45	21.18	21.75	22.46	26.77	21.1	21.13	21.07
Total	53.58	53.04	59.71	56.88	55.65	55.41	56.28	55.79	97.86	53.93	53.80	53.48
Cl wt. %	< 0.01	< 0.01	< 0.01	< 0.01	< 0.01	< 0.01	< 0.01	< 0.01	0.02	< 0.01	< 0.01	< 0.01
CO_2	0.25	0.38	0.59	2.36	0.28	0.08	1.56	0.09	17.9	0.35	0.03	< 0.01
SO_4	56.4	59.8	56	56.4	56.8	57.1	54.3	54.6	2.1	56	58	58
Br	0.02	< 0.5	< 0.5	< 0.5	0.01	0.02	< 0.01	0,01	< 0.5	< 0.5	< 0.5	< 0.5
B	< 0.5	< 0.5	7.6	15.2	< 0.5	< 0.5	< 0.5	< 0.5	74.9	< 0.5	< 0.5	< 0.5
V	< 5	8	15	10	6	< 5	6	9	98	< 5	6	< 5
Ba	6	8	34	41	13	13	68	35	84	5	2	6
Sr	1081	1334	1118	1710	1008	1242	3286	4111	631	771	523	1168
Y	0.7	< 0.5	1.2	< 0.5	1.1	1	1.4	1.5	11.2	0.8	0.8	0.7
Zr	3.4	< 0.1	8.9	2.1	3.5	3.2	3.8	7.9	75.1	4	3.1	3.8
Ga	< 1	< 1	1	< 1	< 1	< 1	< 1	< 1	10	< 1	< 1	< 1
Ge	< 0.5	< 0.5	< 0.5	< 0.5	< 0.5	< 0.5	< 0.5	< 0.5	0.6	< 0.5	< 0.5	< 0.5
As	0.4	0.4	4.5	1.8	0.6	0.3	2.3	1.1	6	0.2	0.2	0.2
Rb	< 0.1	< 0.1	4.6	1.2	< 0.1	< 0.1	< 0.1	1.6	45.2	< 0.1	< 0.1	< 0.1
Nb	< 0.01	< 0.01	0.16	< 0.01	< 0.01	< 0.01	< 0.01	0.2	5.81	0.88	0.57	0.47
Mo	< 2	< 2	< 2	< 2	< 2	< 2	< 2	< 2	3	< 2	< 2	< 2
Ag	< 0.002	0.011	0.005	0.013	< 0.002	0.005	< 0.002	< 0.002	< 0.002	0.004	< 0.002	0.007
In	< 0.1	< 0.1	< 0.1	< 0.1	< 0.1	< 0.1	< 0.1	< 0.1	< 0.1	< 0.1	< 0.1	< 0.1
Sn	< 1	< 1	< 1	< 1	< 1	< 1	< 1	< 1	< 1	< 1	< 1	< 1
Sb	< 0.2	< 0.2	< 0.2	< 0.2	0.5	0.5	0.7	0.3	< 0.2	0.4	0.3	1.5
Cs	< 0.1	< 0.1	0.1	< 0.1	< 0.1	< 0.1	< 0.1	0.1	3.2	< 0.1	< 0.1	< 0.1
Hf	< 0.1	< 0.1	0.2	< 0.1	< 0.1	< 0.1	< 0.1	0.2	1.8	< 0.1	< 0.1	< 0.1
Ta	0.02	< 0.01	< 0.01	< 0.01	0.05	0.06	0.06	0.09	0.47	0.05	0.07	0.04
W	1.6	< 0.5	< 0.5	< 0.5	1.1	1.5	1.7	0.7	< 0.5	1.5	1.5	1.4
Tl	< 0.05	< 0.05	< 0.05	< 0.05	< 0.05	< 0.05	< 0.05	< 0.05	< 0.05	< 0.05	< 0.05	< 0.05
Pb	0.27	0.07	2.12	0.55	0.06	0.09	0.11	0.16	8.89	0.16	0.01	0.05
Bi	< 0.1	< 0.1	< 0.1	< 0.1	< 0.1	< 0.1	< 0.1	< 0.1	< 0.1	0.1	< 0.1	< 0.1
Th	< 0.01	< 0.01	0.88	0.16	0.05	< 0.01	0.09	0.16	3.69	0.08	0.06	0.11
U	0.097	0.094	0.311	0.128	0.052	0.022	0.087	0.18	3.74	0.031	< 0.005	0.024
Cd	0.02	< 0.01	0.03	< 0.01	0.01	0.02	< 0.01	0.01	0.13	0.01	0.02	0.02
Cr	< 20	< 20	20	< 20	< 20	< 20	< 20	< 20	180	< 20	< 20	< 20
Co	0.2	0.2	2.2	0.6	0.2	< 0.1	0.4	0.5	22.1	0.1	< 0.1	0.1
Ni	2.6	2.3	21.4	7.2	2.4	1.6	5	4.3	192	2.4	1.6	2
Cu	0.71	0.87	3.8	1.61	0.73	0.59	1.2	1.25	27.8	0.56	0.68	0.7
Zn	3	0.8	6.8	2.5	1	0.4	1.5	1.9	110	0.7	0.8	0.6

Supplementary Table 1- continue.

	A-1	A-3	A-5	A-6	A-8	A-10	A-11	A-12	A-15	A-16	A-17	A-19	A-20	A-13	A-2
	The Alçıdağ hill section														
	gypsum-rich samples													*marl*	*claystone*
SiO_2 wt. %	0.21	1.45	3.92	0.03	0.26	0.31	0.14	4.07	0.08	0.32	0.02	0.23	0.25	35.25	3.77
Al_2O_3	0.05	0.39	1.05	< 0.01	0.04	0.04	0.04	0.37	0.02	0.07	< 0.01	0.02	0.04	9.54	1.01
$Fe_2O_3^*$	0.04	0.18	0.45	0.01	0.03	0.04	0.03	0.21	0.02	0.05	0.01	0.03	0.03	4.27	0.52
MnO	0.002	0.009	0.008	0.002	0.002	0.002	0.003	0.011	0.002	0.002	0.002	0.002	0.002	0.097	0.043
MgO	0.02	0.74	0.81	0.01	0.11	0.11	0.04	0.9	0.02	0.03	0.02	0.02	0.09	6.26	3.14
CaO	31.86	32	30.83	32.91	33.25	32.65	33.45	31.57	33.37	32.89	33.02	32.7	32.54	13.95	30.31
Na_2O	< 0.01	0.02	0.03	< 0.01	< 0.01	< 0.01	< 0.01	0.03	< 0.01	< 0.01	< 0.01	< 0.01	< 0.01	0.29	0.05
K_2O	0.01	0.11	0.29	< 0.01	0.01	< 0.01	< 0.01	0.08	< 0.01	0.02	< 0.01	< 0.01	0.01	2.06	0.27
TiO_2	0.003	0.017	0.046	< 0.001	0.002	0.002	0.002	0.017	0.001	0.004	< 0.001	0.001	0.002	0.427	0.045
P_2O_5	< 0.01	0.03	0.02	< 0.01	< 0.01	0.02	< 0.01	0.03	< 0.01	0.06	< 0.01	< 0.01	< 0.01	0.14	0.03
LOI	20.94	21.5	21.89	20.91	20.99	21.27	20.87	21.3	20.99	21.46	20.8	20.74	20.81	26.51	24.26
Total	53.16	56.45	59.34	53.89	54.71	54.44	54.59	58.59	54.52	54.91	53.88	53.77	53.78	98.79	63.45
Cl wt. %	< 0.01	< 0.01	< 0.01	< 0.01	< 0.01	< 0.01	< 0.01	< 0.01	< 0.01	< 0.01	< 0.01	< 0.01	< 0.01	0.03	< 0.01
CO_2	0.05	1.63	1.47	0.03	0.12	< 0.01	0.2	1.95	0.07	0.1	0.16	0.26	0.26	13.3	6.84
SO_4	62.4	59.2	56.5	62.5	61.7	56.9	62.1	52.9	61.4	55.8	61.5	61.8	67.3	3.1	46
Br ppm	1.2	< 0.5	1.4	< 0.5	< 0.5	0.01	< 0.5	0.03	< 0.5	0.01	1.7	< 0.5	1.9	0.04	0.03
B	4.2	< 0.5	14.7	1.4	< 0.5	< 0.5	2	1.8	2.1	< 0.5	4.9	3.6	1.3	< 0.5	< 0.5
V	8	11	18	8	9	7	8	9	9	6	7	8	10	110	15
Ba	13	17	31	2	4	3	5	37	3	5	1	2	5	104	53
Sr	1129	1180	1291	1029	1049	949	860	1221	988	329	506	259	1391	915	992
Y	< 0.5	0.7	1.3	< 0.5	< 0.5	< 0.5	< 0.5	1.6	< 0.5	< 0.5	< 0.5	< 0.5	< 0.5	10.3	3.1
Zr	< 0.1	2.9	7.8	< 0.1	0.3	3.1	< 0.1	5	< 0.1	3.2	< 0.1	< 0.1	< 0.1	63.8	8.7
Ga	< 1	< 1	1	< 1	< 1	< 1	< 1	< 1	< 1	< 1	< 1	< 1	< 1	9	< 1
Ge	< 0.5	< 0.5	< 0.5	< 0.5	< 0.5	< 0.5	< 0.5	< 0.5	< 0.5	< 0.5	< 0.5	< 0.5	< 0.5	0.6	< 0.5
As	0.8	1.3	1.6	0.3	0.5	1	0.6	1.1	0.5	0.3	0.2	0.4	0.5	15.1	1.7
Rb	< 0.1	2.3	6.9	< 0.1	< 0.1	< 0.1	< 0.1	1.6	< 0.1	< 0.1	< 0.1	< 0.1	< 0.1	51.5	5.4
Nb	0.79	1.04	1.37	0.7	0.51	< 0.01	0.4	< 0.01	0.42	< 0.01	0.4	0.44	0.34	4.69	0.21
Mo	< 2	< 2	< 2	< 2	< 2	< 2	< 2	< 2	< 2	< 2	< 2	< 2	< 2	2	< 2
Ag	0.01	0.009	0.008	0.008	0.007	0.003	< 0.002	< 0.002	< 0.002	< 0.002	< 0.002	0.007	0.003	0.006	< 0.002
In	< 0.1	< 0.1	< 0.1	< 0.1	< 0.1	< 0.1	< 0.1	< 0.1	< 0.1	< 0.1	< 0.1	< 0.1	< 0.1	< 0.1	< 0.1
Sn	< 1	< 1	< 1	< 1	< 1	< 1	< 1	< 1	< 1	< 1	< 1	< 1	< 1	< 1	< 1
Sb	< 0.2	< 0.2	< 0.2	< 0.2	< 0.2	0.4	< 0.2	0.5	< 0.2	0.4	< 0.2	< 0.2	< 0.2	0.7	0.3
Cs	< 0.1	< 0.1	0.2	< 0.1	< 0.1	< 0.1	< 0.1	0.1	< 0.1	< 0.1	< 0.1	< 0.1	< 0.1	4.1	0.3
Hf	< 0.1	< 0.1	0.2	< 0.1	< 0.1	< 0.1	< 0.1	< 0.1	< 0.1	< 0.1	< 0.1	< 0.1	< 0.1	1.6	< 0.1
Ta	< 0.01	< 0.01	0.04	< 0.01	< 0.01	0.05	< 0.01	0.06	< 0.01	0.05	< 0.01	< 0.01	< 0.01	0.38	0.08
W	< 0.5	< 0.5	< 0.5	< 0.5	< 0.5	1.1	< 0.5	1.7	< 0.5	1.4	< 0.5	< 0.5	< 0.5	1.1	1.6
Tl	< 0.05	< 0.05	< 0.05	< 0.05	< 0.05	< 0.05	< 0.05	< 0.05	< 0.05	< 0.05	< 0.05	< 0.05	< 0.05	0.18	< 0.05
Pb	0.3	0.38	0.66	0.02	0.34	0.4	0.22	0.35	0.1	0.1	0.02	0.04	0.19	6.73	0.69
Bi	< 0.1	< 0.1	< 0.1	< 0.1	< 0.1	< 0.1	< 0.1	< 0.1	< 0.1	< 0.1	< 0.1	< 0.1	< 0.1	< 0.1	< 0.1
Th	0.02	0.19	0.53	< 0.01	0.01	< 0.01	0.01	0.18	< 0.01	< 0.01	< 0.01	< 0.01	0.01	4.27	0.41
U	0.078	0.148	0.306	< 0.005	0.101	0.651	0.047	0.227	0.027	0.121	< 0.005	0.052	0.361	1.7	0.206
Cd	< 0.01	< 0.01	0.02	< 0.01	0.01	0.01	< 0.01	< 0.01	0.02	0.01	< 0.01	0.01	< 0.01	0.04	0.03
Cr	< 20	< 20	< 20	< 20	< 20	< 20	< 20	< 20	< 20	< 20	< 20	< 20	< 20	60	< 20
Co	0.3	0.8	1.4	< 0.1	0.2	0.2	0.2	0.8	0.2	0.2	0.1	< 0.1	0.2	10.5	1.4
Ni	3.4	6.8	6.3	1.6	2.8	2.7	2.9	6	2.6	2.2	2.3	1.1	2.9	64.4	10.3
Cu	0.99	2.57	6.07	0.48	0.82	0.73	0.83	2.49	0.71	0.83	0.51	0.41	0.93	42.7	5.78
Zn	5.1	2.9	6.6	0.6	1	0.8	1.7	6	1.6	1	1	0.6	1.1	46.4	4.7

Supplementary Table 1- continue.

	K-1	K-3	K-4	K-5	K-9	K-10	K-11	K-12	K-14	K-15	K-7	K-13a	K-13b	K-13c	K-8	K-17	K-19a
	The Gümüşseren section																
		gypsum-rich samples									*marl*						*claystone*
SiO_2 wt. %	0.85	0.03	0.05	0.14	0.24	1.25	2.17	0.39	0.12	0.25	15.75	31.7	15.73	7.16	10.62	7.86	52.95
Al_2O_3	0.2	< 0.01	< 0.01	0.04	0.05	0.23	0.52	0.12	0.04	0.07	4.08	9.49	4.5	1.97	3.01	1.79	9.74
$Fe_2O_3^*$	0.11	0.01	0.02	0.03	0.03	0.11	0.28	0.1	0.03	0.07	2.29	6.54	3.23	2.53	1.71	0.81	7.08
MnO	0.005	0.002	0.002	0.002	0.003	0.004	0.005	0.006	0.003	0.003	0.144	0.085	0.137	0.166	0.11	0.069	0.037
MgO	0.08	0.04	< 0.01	0.03	0.04	0.29	0.18	0.69	0.08	0.3	1.94	7.07	12.64	15.29	1.45	1.15	8.08
CaO	32.68	32.58	32.32	32.76	33	32.54	31.29	31.13	32.29	33.04	28.68	11.22	22.54	28.07	25.29	46.76	2.31
Na_2O	0.01	< 0.01	< 0.01	0.01	< 0.01	< 0.01	0.02	0.02	0.01	0.01	0.1	0.95	0.39	0.16	0.08	0.27	0.67
K_2O	0.04	< 0.01	< 0.01	< 0.01	0.01	0.06	0.11	0.04	0.01	0.02	0.82	1.96	1.04	0.8	0.62	0.3	1.8
TiO_2	0.01	< 0.001	< 0.001	< 0.001	0.002	0.01	0.023	0.007	0.002	0.004	0.227	0.814	0.273	0.116	0.178	0.094	0.473
P_2O_5	0.01	< 0.01	< 0.01	0.02	< 0.01	< 0.01	0.01	< 0.01	< 0.01	< 0.01	0.09	0.12	0.11	0.07	0.08	0.12	0.1
LOI	21.34	20.9	21.11	20.77	20.7	21.16	22.1	20.48	20.86	20.91	26.25	25.15	32.53	39.72	30.38	39.18	16.8
Total	55.33	53.57	53.50	53.81	54.07	55.66	56.71	52.98	53.46	54.7	80.36	95.09	93.11	96.04	73.53	98.40	100
Cl wt. %	0.01	< 0.01	0.02	< 0.01	< 0.01	< 0.01	< 0.01	< 0.01	< 0.01	< 0.01	< 0.01	0.03	0.03	0.04	< 0.01	< 0.01	0.01
CO_2	0.39	0.11	< 0.01	0.18	0.17	0.73	0.32	1.7	0.24	0.85	16.7	12.6	27.8	39.8	22.2	37.1	2.4
SO_4	59.5	61.4	58.1	59.9	61.6	59.7	59.2	59.2	61.2	60.2	18.1	11.1	7.7	2.2	9.9	< 0.3	< 0.3
Br ppm	< 0.5	1.4		< 0.5	< 0.5	< 0.5	< 0.5	< 0.5	< 0.5	< 0.5	< 0.5	4.8	4.2	6	0.41	0.09	< 0.5
B	1.3	5.8	1.5	6	0.8	5.3	< 0.5	0.9	2.5	2.9	37.7	188	115	53.5	< 0.5	3.5	76.6
V	10	7	< 5	7	7	9	13	10	8	9	51	166	68	37	37	25	100
Ba	16	2	4	19	2	16	39	305	3	4	488	78	41	19	292	676	131
Sr	1572	1045	1058	4445	701	1267	2470	13100	1231	228	60090	223	189	181	> 10000	509	169
Y	< 0.5	< 0.5	1	0.5	< 0.5	< 0.5	< 0.5	< 0.5	< 0.5	< 0.5	7.5	10.7	8.3	7.6	6.4	3.4	10.9
Zr	1.3	< 0.1	4.1	0.2	< 0.1	0.9	3.3	0.6	< 0.1	< 0.1	46.5	82.6	36.4	15.8	38.9	19.3	77.4
Ga	< 1	< 1	< 1	< 1	< 1	< 1	< 1	< 1	< 1	< 1	4	11	5	2	4	2	10
Ge	< 0.5	< 0.5	< 0.5	< 0.5	< 0.5	< 0.5	< 0.5	< 0.5	< 0.5	< 0.5	< 0.5	1.2	< 0.5	< 0.5	< 0.5	< 0.5	1.7
As	0.8	0.7	0.2	0.7	0.6	1	1.1	1.8	0.6	0.5	1	25.7	5.8	3.4	14.2	1.5	2.2
Rb	0.5	< 0.1	< 0.1	< 0.1	< 0.1	0.7	2.4	0.1	< 0.1	< 0.1	22.7	49.8	29.1	11.7	16.8	12	54.3
Nb	< 0.01	< 0.01	< 0.01	< 0.01	< 0.01	< 0.01	< 0.01	< 0.01	< 0.01	< 0.01	4.51	9.66	2.79	1.04	4.61	1.33	6.74
Mo	< 2	< 2	< 2	< 2	< 2	< 2	< 2	< 2	< 2	< 2	< 2	25	2	< 2	6	< 2	< 2
Ag	0.01	0.013	< 0.002	0.012	0.011	0.005	0.018	0.016	0.018	0.004	0.019	< 0.002	0.011	0.02	0.013	< 0.002	< 0.002
In	< 0.1	< 0.1	< 0.1	< 0.1	< 0.1	< 0.1	< 0.1	< 0.1	< 0.1	< 0.1	< 0.1	< 0.1	< 0.1	< 0.1	< 0.1	< 0.1	< 0.1
Sn	< 1	< 1	< 1	< 1	< 1	< 1	< 1	< 1	< 1	< 1	< 1	1	< 1	< 1	< 1	< 1	< 1
Sb	< 0.2	< 0.2	0.6	< 0.2	< 0.2	< 0.2	< 0.2	< 0.2	< 0.2	< 0.2	< 0.2	1.9	< 0.2	< 0.2	0.8	0.5	0.7
Cs	< 0.1	< 0.1	< 0.1	< 0.1	< 0.1	< 0.1	< 0.1	< 0.1	< 0.1	< 0.1	1.6	4.1	2.4	0.8	1.3	1.3	3.5
Hf	< 0.1	< 0.1	< 0.1	< 0.1	< 0.1	< 0.1	< 0.1	< 0.1	< 0.1	< 0.1	1.1	1.8	0.9	0.4	1	0.4	1.8
Ta	< 0.01	< 0.01	0.05	< 0.01	< 0.01	< 0.01	< 0.01	< 0.01	< 0.01	< 0.01	0.22	0.61	0.16	0.02	0.34	0.16	0.45
W	< 0.5	< 0.5	1.7	< 0.5	< 0.5	< 0.5	< 0.5	< 0.5	< 0.5	< 0.5	< 0.5	< 0.5	< 0.5	< 0.5	1.5	1.4	1.1
Tl	< 0.05	< 0.05	< 0.05	< 0.05	< 0.05	< 0.05	< 0.05	< 0.05	< 0.05	< 0.05	0.14	0.2	< 0.05	< 0.05	0.13	0.06	0.13
Pb	0.61	0.03	0.03	0.05	0.08	0.2	0.41	0.77	0.2	0.12	7.37	6.48	3.64	2.19	6.42	2.42	8.26
Bi	< 0.1	< 0.1	< 0.1	< 0.1	< 0.1	< 0.1	< 0.1	< 0.1	< 0.1	< 0.1	< 0.1	< 0.1	< 0.1	< 0.1	< 0.1	< 0.1	0.2
Th	0.08	0.01	< 0.01	0.06	< 0.01	0.07	0.21	0.02	< 0.01	< 0.01	2.55	3.18	1.57	0.8	1.88	1	5.15
U	0.091	< 0.005	0.047	0.074	0.023	0.069	0.117	0.419	0.168	0.052	3.82	4.83	2.88	1.08	3.67	1.08	0.948
Cd	0.02	0.01	< 0.01	0.01	< 0.01	< 0.01	< 0.01	0.01	0.01	0.03	0.37	0.08	0.06	0.06	0.41	0.09	0.05
Cr	< 20	< 20	< 20	< 20	< 20	< 20	< 20	< 20	< 20	< 20	50	280	100	50	50	70	630
Co	0.6	< 0.1	< 0.1	0.1	0.2	0.4	0.7	0.4	0.2	0.3	11.8	37.4	14.4	7.3	9.5	2.8	49.4
Ni	5.7	1.6	1.4	1.9	2.1	3.1	4.9	4.8	2.7	3.2	120	337	136	61.2	112	35.7	848
Cu	1.5	0.49	0.54	0.53	0.87	1.45	2.34	1.71	0.74	0.71	16	60.6	33.1	15.5	15.5	7.49	31.9
Zn	2	0.7	0.4	1.4	2.1	2.2	4.3	2.3	1.8	1.8	24.3	43.4	22.5	10.1	33.2	14.2	72.4

All Fe as $Fe_2O_3^*$; LOI is loss on ignition

Supplementary Table 2- Rare earth element (REE, ppm) compositions of the Aşkale evaporites. Normalizing values (MuQ; Mud of Queensland-alluvial sediment composite) from Kamber et al. (2005).

	D1-1	D1-2	D1-5	D1-10	D1-11	D1-13	D1-15	D1-18	D1-25	D1-28	D1-30	D1-22	D1-24	D1-21
	The Pırnakapan Section													
	gypsum-rich samples											*anhydrite-rich samples*		*limestone*
La	0.850	1.300	0.380	0.260	0.080	0.230	0.560	0.710	0.180	0.090	0.640	0.180	0.480	1.470
Ce	1.620	2.100	0.740	0.500	0.220	0.420	0.980	1.280	0.330	0.190	1.120	0.360	1.100	2.680
Pr	0.180	0.180	0.080	0.050	0.020	0.030	0.100	0.170	0.030	0.010	0.120	0.040	0.130	0.330
Nd	0.550	0.630	0.280	0.130	0.110	< 0.05	0.280	0.580	< 0.05	< 0.05	0.280	0.070	0.510	1.260
Sm	0.090	0.120	< 0.01	0.020	< 0.01	< 0.01	< 0.01	0.060	< 0.01	< 0.01	0.020	0.020	0.120	0.270
Eu	0.019	0.028	< 0.005	< 0.005	0.009	< 0.005	< 0.005	0.007	< 0.005	< 0.005	< 0.005	0.006	0.015	0.056
Gd	0.140	0.120	0.040	0.020	0.030	< 0.01	0.030	0.060	< 0.01	< 0.01	0.050	0.020	0.150	0.240
Tb	0.020	0.010	< 0.01	< 0.01	< 0.01	< 0.01	< 0.01	< 0.01	< 0.01	< 0.01	< 0.01	< 0.01	0.020	0.040
Dy	0.090	0.080	0.020	0.020	0.030	< 0.01	0.010	0.050	< 0.01	< 0.01	0.020	0.020	0.110	0.250
Ho	0.020	0.010	< 0.01	< 0.01	< 0.01	< 0.01	< 0.01	0.010	< 0.01	< 0.01	< 0.01	< 0.01	0.020	0.050
Er	0.060	0.050	0.020	0.010	0.020	< 0.01	0.010	0.040	< 0.01	< 0.01	0.020	0.010	0.040	0.130
Tm	0.008	0.006	< 0.005	< 0.005	< 0.005	< 0.005	< 0.005	< 0.005	< 0.005	< 0.005	< 0.005	< 0.005	0.007	0.022
Yb	0.040	0.030	< 0.01	< 0.01	0.010	< 0.01	< 0.01	0.020	< 0.01	< 0.01	0.010	0.020	0.050	0.150
Lu	0.004	< 0.002	< 0.002	< 0.002	< 0.002	< 0.002	< 0.002	< 0.002	< 0.002	< 0.002	< 0.002	< 0.002	0.007	0.023
La_N / Lu_N	3.204	-	-	-	-	-	-	-	-	-	-	-	1.034	0.964
Ce_N / Ce^*	0.961	0.964	0.984	1.011	1.283	1.112	0.949	0.859	1.022	1.353	0.930	0.987	1.027	0.895
Eu_N / Eu^*	0.690	0.982	-	-	-	-	-	0.491	-	-	-	1.263	0.466	0.927

	D1-32	D2-4	D3-1	D3-2	D3-5	D3-4	D3-6	28	D2-2	K-22	K-25	K-24
	The Pırnakapan Section									The Kemerkaya Section		
	gypsum-rich samples								*claystone*	*gypsum-rich samples*		
La	0.51	0.17	1.97	0.46	0.23	0.19	0.38	0.69	11.8	0.36	0.23	0.84
Ce	0.6	0.31	3.71	0.94	0.47	0.29	0.83	1.28	22.8	0.66	0.38	1.55
Pr	0.03	0.02	0.4	0.1	0.06	0.03	0.09	0.13	2.7	0.07	0.05	0.18
Nd	0.12	< 0.05	1.38	0.36	0.24	0.1	0.31	0.43	10.4	0.31	0.1	0.71
Sm	< 0.01	< 0.01	0.25	0.07	0.03	0.04	0.07	0.19	2.16	0.07	0.04	0.14
Eu	0.017	< 0.005	0.036	0.021	0.017	0.013	0.024	0.037	0.58	0.02	0.01	0.024
Gd	0.04	< 0.01	0.19	0.07	0.05	0.03	0.09	0.16	2.06	0.06	< 0.01	0.06
Tb	< 0.01	< 0.01	0.03	< 0.01	< 0.01	< 0.01	0.02	0.02	0.34	< 0.01	< 0.01	0.01
Dy	0.03	< 0.01	0.16	0.06	0.05	0.03	0.09	0.12	1.92	0.03	< 0.01	0.05
Ho	< 0.01	< 0.01	0.04	0.01	< 0.01	< 0.01	0.01	0.02	0.38	< 0.01	< 0.01	< 0.01
Er	0.01	< 0.01	0.1	0.04	0.01	< 0.01	0.03	0.05	1.12	0.03	< 0.01	0.03
Tm	< 0.005	< 0.005	0.012	0.007	< 0.005	< 0.005	< 0.005	0.008	0.17	< 0.005	< 0.005	0.005
Yb	< 0.01	< 0.01	0.06	0.04	0.02	< 0.01	0.06	0.07	1.12	< 0.01	< 0.01	< 0.01
Lu	0.004	< 0.002	0.007	0.005	0.004	< 0.002	0.002	0.012	0.17	0.002	< 0.002	0.003
La_N / Lu_N	1.922	-	4.243	1.387	0.867	-	2.864	0.867	1.047	2.713	-	4.220
Ce_N / Ce^*	0.878	1.148	0.967	1.018	0.933	0.869	1.046	0.984	0.94	0.960	0.823	0.926
Eu_N / Eu^*	-	-	0.693	1.263	1.772	1.573	1.257	0.893	1.158	1.299	-	1.027

Supplementary Table 2- continue.

	A-1	A-3	A-5	A-6	A-8	A-10	A-11	A-12	A-15	A-16	A-17	A-19	A-20	A-13	A-2
	The Alçıdağ hill section														
	gypsum-rich samples													*marl*	*claystone*
La	0.33	1.18	1.7	0.16	0.3	0.13	0.15	1	0.26	0.15	0.12	0.21	0.22	13.2	2.72
Ce	0.51	2.07	3.24	0.28	0.55	0.27	0.31	1.98	0.43	0.32	0.19	0.36	0.42	25.3	5.4
Pr	0.06	0.23	0.37	0.02	0.05	0.04	0.03	0.22	0.04	0.04	0.01	0.03	0.04	2.81	0.62
Nd	0.13	0.76	1.35	< 0.05	0.11	0.12	< 0.05	0.88	< 0.05	0.12	< 0.05	< 0.05	0.08	10.6	2.1
Sm	0.02	0.17	0.23	< 0.01	< 0.01	0.05	< 0.01	0.14	< 0.01	0.03	< 0.01	< 0.01	< 0.01	2.46	0.43
Eu	0.006	0.047	0.061	< 0.005	< 0.005	0.011	< 0.005	0.05	< 0.005	0.016	< 0.005	< 0.005	< 0.005	0.643	0.146
Gd	0.02	0.14	0.26	< 0.01	< 0.01	0.02	< 0.01	0.13	< 0.01	0.03	< 0.01	< 0.01	< 0.01	2.11	0.45
Tb	< 0.01	0.02	0.03	< 0.01	< 0.01	< 0.01	< 0.01	0.03	< 0.01	< 0.01	< 0.01	< 0.01	< 0.01	0.33	0.07
Dy	0.02	0.1	0.21	< 0.01	< 0.01	0.04	< 0.01	0.17	< 0.01	0.03	< 0.01	< 0.01	< 0.01	1.9	0.44
Ho	< 0.01	0.02	0.04	< 0.01	< 0.01	< 0.01	< 0.01	0.03	< 0.01	< 0.01	< 0.01	< 0.01	< 0.01	0.37	0.09
Er	0.01	0.07	0.13	< 0.01	< 0.01	0.02	< 0.01	0.07	< 0.01	0.01	< 0.01	< 0.01	< 0.01	1.05	0.25
Tm	< 0.005	0.01	0.018	< 0.005	< 0.005	< 0.005	< 0.005	< 0.005	< 0.005	< 0.005	< 0.005	< 0.005	< 0.005	0.155	< 0.005
Yb	0.02	0.07	0.11	< 0.01	< 0.01	0.02	< 0.01	0.11	< 0.01	< 0.01	< 0.01	< 0.01	< 0.01	1.02	0.22
Lu	0.002	0.012	0.019	< 0.002	< 0.002	< 0.002	< 0.002	0.011	< 0.002	< 0.002	< 0.002	< 0.002	< 0.002	0.164	0.038
La_N / Lu_N	2.488	1.483	1.349	-	-	-	-	1.370	-	-	-	-	-	1.213	1.079
Ce_N / Ce^*	0.832	0.917	0.949	1.081	1.022	0.870	1.069	0.981	0.95	0.964	1.097	1.012	1.028	0.964	0.968
Eu_N / Eu^*	1.263	1.281	1.046	-	-	1.346	-	1.562	-	2.245	-	-	-	1.188	1.396

	K-1	K-3	K-4	K-5	K-9	K-10	K-11	K-12	K-14	K-15	K-7	K-13a	K-13b	K-13c	K-8	K-17	K-19a
	The Gümüşseren section																
		gypsum-rich samples									*marl*						*claystone*
La	0.3	0.08	0.18	0.66	0.17	0.45	0.64	0.34	0.08	0.19	9.81	9.57	6.96	8.48	8.45	3.62	14.9
Ce	0.66	0.18	0.33	1.42	0.3	0.8	1.28	0.64	0.2	0.33	19.9	20.6	13.2	14.3	17	7.74	28.6
Pr	0.07	< 0.01	0.04	0.17	0.02	0.09	0.14	0.05	< 0.01	0.03	2.11	2.4	1.59	1.69	1.86	0.82	3.3
Nd	0.14	< 0.05	0.21	0.61	< 0.05	0.18	0.49	0.18	< 0.05	< 0.05	8.19	9.43	6.2	6.52	7.15	3.16	12.4
Sm	< 0.01	< 0.01	0.07	0.13	< 0.01	0.01	0.05	< 0.01	< 0.01	< 0.01	1.71	2.1	1.29	1.22	1.46	0.83	2.67
Eu	< 0.005	< 0.005	0.016	0.012	< 0.005	< 0.005	< 0.005	< 0.005	< 0.005	< 0.005	0.393	0.574	0.366	0.336	0.355	0.24	0.628
Gd	0.01	< 0.01	0.03	0.13	< 0.01	0.02	0.09	0.02	< 0.01	< 0.01	1.32	2.11	1.41	1.34	1.28	0.63	2.4
Tb	< 0.01	< 0.01	< 0.01	0.01	< 0.01	< 0.01	< 0.01	< 0.01	< 0.01	< 0.01	0.22	0.34	0.22	0.21	0.21	0.11	0.36
Dy	< 0.01	< 0.01	0.01	0.09	< 0.01	0.02	0.05	< 0.01	< 0.01	< 0.01	1.37	2.33	1.25	1.13	1.22	0.63	2.26
Ho	< 0.01	< 0.01	< 0.01	0.02	< 0.01	< 0.01	< 0.01	< 0.01	< 0.01	< 0.01	0.27	0.47	0.27	0.22	0.24	0.12	0.44
Er	< 0.01	< 0.01	0.02	0.05	< 0.01	< 0.01	0.02	< 0.01	< 0.01	< 0.01	0.79	1.3	0.82	0.66	0.66	0.33	1.24
Tm	< 0.005	< 0.005	< 0.005	0.007	< 0.005	< 0.005	< 0.005	< 0.005	< 0.005	< 0.005	0.118	0.198	0.123	0.092	0.094	0.045	0.191
Yb	< 0.01	< 0.01	< 0.01	0.04	< 0.01	< 0.01	0.02	< 0.01	< 0.01	< 0.01	0.77	1.31	0.86	0.55	0.61	0.3	1.26
Lu	< 0.002	< 0.002	< 0.002	0.006	< 0.002	< 0.002	< 0.002	< 0.002	< 0.002	< 0.002	0.123	0.213	0.138	0.083	0.096	0.053	0.214
La_N / Lu_N	-	-	-	1.658	-	-	-	-	-	-	1.202	0.677	0.76	1.54	1.327	1.029	1.05
Ce_N / Ce^*	1.061	-	0.904	0.989	1.111	0.919	0.994	1.1	-	0.988	1.016	1.002	0.924	0.873	0.997	1.045	0.948
Eu_N / Eu^*	-	-	1.369	0.389	-	-	-	-	-	-	1.098	1.148	1.139	1.103	1.094	1.392	1.045

$Ce_N / Ce^* = Ce_N / ((La_N + Pr_N) / 2)$, $Eu_N / Eu^* = Eu_N / ((Sm_N + Gd_N) / 2)$, Normalizing values (MuQ; Mud of Queensland-alluvial sediment composite) from Kamber et al. (2005).

Supplementary Table 3- Calculated mean, standard deviation, and correlation coefficients of the Aşkale evaporite samples (n=42). Shaded correlation coefficients are significant at p<0.01 value.

	Mean.	Std.Dev.	SiO_2	Al_2O_3	$Fe_2O_3^*$	MnO	MgO	CaO	Na_2O	K_2O	TiO_2	P_2O_5	AK	CO_2	SO_4	B	V	Ba	Sr
SiO_2	4.37	9.99	1.00																
Al_2O_3	1.08	2.47	0.97	1.00															
$Fe_2O_3^*$	1.08	1.55	0.97	0.97	1.00														
MnO	1.08	0.04	0.59	0.66	0.67	1.00													
MgO	1.08	2.94	0.61	0.62	0.71	0.80	1.00												
CaO	1.08	6.69	-0.82	-0.80	-0.82	-0.43	-0.58	1.00											
Na_2O	1.08	0.18	0.88	0.91	0.94	0.56	0.62	-0.70	1.00										
K_2O	1.08	0.49	0.95	0.98	0.97	0.72	0.71	-0.79	0.89	1.00									
TiO_2	1.08	0.15	0.91	0.96	0.96	0.64	0.61	-0.77	0.96	0.95	1.00								
P_2O_5	1.08	0.03	0.81	0.85	0.82	0.81	0.67	-0.52	0.78	0.87	0.82	1.00							
LOI	1.08	5.77	0.21	0.26	0.27	0.60	0.48	-0.04	0.25	0.33	0.26	0.50	1.00						
CO_2	1.08	9.89	0.37	0.43	0.44	0.78	0.63	0.00	0.42	0.49	0.41	0.69	0.82	1.00					
SO_4	1.08	20.75	-0.33	-0.48	-0.44	-0.69	-0.52	0.30	-0.35	-0.54	-0.50	-0.50	-0.55	-0.59	1.00				
B	1.08	31.48	0.67	0.73	0.81	0.58	0.69	-0.61	0.89	0.75	0.85	0.62	0.23	0.41	-0.45	1.00			
V	1.08	37.79	0.64	0.68	0.68	0.43	0.42	-0.57	0.67	0.68	0.71	0.61	0.18	0.25	-0.39	0.58	1.00		
Ba	1.08	117.69	0.31	0.31	0.27	0.51	0.12	0.02	0.26	0.30	0.28	0.57	0.45	0.56	-0.06	0.11	0.13	1.00	
Sr	1.08	8093.36	0.09	0.10	0.08	0.34	-0.02	0.05	-0.04	0.11	0.08	0.17	0.15	0.22	-0.26	0.05	0.02	0.52	1.00
Y	1.08	3.02	0.92	0.95	0.95	0.84	0.76	-0.74	0.86	0.96	0.92	0.90	0.41	0.59	-0.60	0.74	0.66	0.38	0.17
Zr	1.08	20.15	0.95	0.98	0.97	0.70	0.60	-0.78	0.91	0.96	0.97	0.86	0.29	0.45	-0.50	0.75	0.70	0.38	0.17
As	1.08	4.19	0.61	0.72	0.70	0.55	0.46	-0.56	0.72	0.76	0.82	0.67	0.23	0.38	-0.58	0.67	0.55	0.19	-0.07
Rb	1.08	13.42	0.98	1.00	0.98	0.68	0.65	-0.79	0.91	0.99	0.96	0.87	0.28	0.45	-0.47	0.74	0.68	0.33	0.10
Nb	1.08	1.90	0.89	0.93	0.94	0.65	0.54	-0.76	0.90	0.92	0.96	0.80	0.25	0.40	-0.47	0.79	0.69	0.36	0.18
Ag	1.08	0.01	-0.10	-0.09	-0.07	0.05	0.01	0.22	-0.09	-0.07	-0.09	-0.05	-0.39	0.00	0.06	-0.03	-0.14	-0.01	0.09
Hf	1.08	0.45	0.95	0.99	0.96	0.69	0.59	-0.78	0.89	0.96	0.96	0.85	0.27	0.44	-0.50	0.73	0.68	0.37	0.17
Pb	1.08	2.25	0.91	0.93	0.90	0.75	0.55	-0.70	0.81	0.90	0.88	0.84	0.33	0.51	-0.52	0.63	0.60	0.50	0.30
Bi	1.08	0.02	0.44	0.31	0.37	0.00	0.19	-0.42	0.29	0.28	0.23	0.14	-0.10	-0.06	0.25	0.18	0.14	0.05	-0.03
Th	1.08	1.11	0.98	0.98	0.95	0.65	0.58	-0.79	0.84	0.96	0.90	0.84	0.25	0.42	-0.41	0.63	0.63	0.39	0.18
U	1.08	1.11	0.65	0.75	0.74	0.77	0.50	-0.43	0.73	0.76	0.81	0.78	0.50	0.68	-0.74	0.72	0.53	0.48	0.39
Cd	1.08	0.07	0.37	0.41	0.39	0.69	0.20	-0.22	0.27	0.40	0.40	0.53	0.37	0.50	-0.49	0.24	0.24	0.64	0.57
Co	1.08	8.74	0.94	0.90	0.96	0.53	0.61	-0.81	0.92	0.87	0.90	0.71	0.15	0.32	-0.26	0.81	0.63	0.25	0.07
Ni	1.08	122.02	0.87	0.77	0.85	0.37	0.52	-0.76	0.78	0.74	0.73	0.58	0.05	0.20	-0.02	0.64	0.51	0.22	0.04
Cu	1.08	11.53	0.88	0.94	0.94	0.72	0.72	-0.77	0.91	0.97	0.97	0.85	0.32	0.47	-0.57	0.84	0.69	0.26	0.06
Zn	1.08	18.85	0.89	0.91	0.87	0.56	0.46	-0.68	0.83	0.84	0.84	0.72	0.22	0.38	-0.42	0.60	0.57	0.29	0.06
La	1.08	3.60	0.93	0.94	0.94	0.81	0.71	-0.75	0.80	0.95	0.87	0.87	0.38	0.57	-0.53	0.64	0.61	0.42	0.22
Ce	1.08	7.03	0.94	0.95	0.94	0.80	0.69	-0.75	0.82	0.95	0.89	0.88	0.37	0.56	-0.53	0.66	0.62	0.44	0.23

Supplementary Table 3- continue.

	Y	Zr	As	Rb	Nb	Ag	Hf	Pb	Bi	Th	U	Cd	Co	Ni	Cu	Zn	La	Ce
Y	1.00																	
Zr	0.96	1.00																
As	0.69	0.73	1.00															
Rb	0.96	0.98	0.71	1.00														
Nb	0.90	0.96	0.78	0.93	1.00													
Ag	-0.05	-0.09	0.06	-0.08	-0.08	1.00												
Hf	0.96	0.99	0.72	0.98	0.96	-0.06	1.00											
Pb	0.94	0.96	0.65	0.93	0.92	-0.04	0.97	1.00										
Bi	0.24	0.29	-0.03	0.31	0.28	-0.05	0.28	0.26	1.00									
Th	0.94	0.97	0.64	0.98	0.91	-0.07	0.97	0.96	0.37	1.00								
U	0.81	0.82	0.74	0.75	0.84	-0.03	0.81	0.84	0.00	0.72	1.00							
Cd	0.54	0.53	0.40	0.42	0.56	0.05	0.53	0.68	-0.01	0.49	0.74	1.00						
Co	0.86	0.91	0.60	0.90	0.90	-0.08	0.90	0.84	0.47	0.89	0.66	0.35	1.00					
Ni	0.72	0.77	0.38	0.78	0.76	-0.08	0.77	0.73	0.61	0.81	0.46	0.27	0.95	1.00				
Cu	0.92	0.93	0.85	0.95	0.92	-0.06	0.93	0.84	0.19	0.88	0.79	0.38	0.85	0.67	1.00			
Zn	0.87	0.91	0.54	0.90	0.84	-0.08	0.92	0.91	0.29	0.91	0.70	0.45	0.82	0.72	0.76	1.00		
La	0.98	0.95	0.63	0.95	0.89	-0.04	0.95	0.96	0.33	0.97	0.77	0.58	0.85	0.75	0.87	0.87	1.00	
Ce	0.98	0.96	0.66	0.96	0.91	-0.04	0.96	0.97	0.32	0.97	0.79	0.60	0.86	0.75	0.89	0.88	1.00	1.00

Std.Dev., standard deviation; All Fe as $Fe_2O_3^*$; LOI is loss on ignition